Hierarchical architecture of dopaminergic circuits enables second-order conditioning in *Drosophila*

Daichi Yamada[1], Daniel Bushey[2], Li Feng[2], Karen Hibbard[2], Megan Sammons[2], Jan Funke[2], Ashok Litwin-Kumar[3], Toshihide Hige[1,4,5]*, Yoshinori Aso[2]*

1: Department of Biology, University of North Carolina at Chapel Hill, Chapel Hill, United States

2: Janelia Research Campus, Howard Hughes Medical Institute, Ashburn, United States

3: Department of Neuroscience, Columbia University, New York, United States

4: Department of Cell Biology and Physiology, University of North Carolina at Chapel Hill, Chapel Hill, United States

5: Integrative Program for Biological and Genome Sciences, University of North Carolina at Chapel Hill, Chapel Hill, United States

* Contact Info

hige@email.unc.edu

asoy@janelia.hhmi.org

Abstract

Dopaminergic neurons with distinct projection patterns and physiological properties compose memory subsystems in a brain. However, it is poorly understood whether or how they interact during complex learning. Here, we identify a feedforward circuit formed between dopamine subsystems and show that it is essential for second-order conditioning, an ethologically important form of higher-order associative learning. The *Drosophila* mushroom body comprises a series of dopaminergic compartments, each of which exhibits distinct memory dynamics. We find that a slow and stable memory compartment can serve as an effective "teacher" by instructing other faster and transient memory compartments via a single key interneuron, which we identify by connectome analysis and neurotransmitter prediction. This excitatory interneuron acquires enhanced response to reward-predicting odor after first-order conditioning and, upon activation, evokes dopamine release in the "student" compartments. These hierarchical connections between dopamine subsystems explain distinct properties of first- and second-order memory long known by behavioral psychologists.

Introduction

Knowledge about order and regularities in environments is crucial for animal survival. Although direct temporal correlation between stimuli and rewards is a primary drive for associative learning, animals are also capable of learning indirect relations between stimuli and rewards in many real-life situations. For example, bumble bees, who have prior foraging experience with other bees, can learn to visit a flower of a particular color without tasting nectar just by watching other bees sitting on flowers of that color (Avarguès-Weber and Chittka, 2014a; Worden and Papaj, 2005a). In the case of humans, some TV commercials are intended to condition consumers to associate items with the positive valence that has been already associated with popular cartoon characters. In both cases,

learning depends on the valence of stimuli (i.e. sight of other bees or cartoon characters) that is acquired through prior experience. Although such higher-order associative learning is widely observed across species and ethologically important, its circuit mechanisms are poorly understood compared to those of simpler forms of associative learning.

Second-order conditioning is a major form of higher-order associative learning. In this learning paradigm, an initially neutral stimulus is paired with reward or punishment; that stimulus, which is now predictive of reward/punishment, then serves as an effective reinforcer when learning about a new stimulus. Since Pavlov's classic experiment with dogs (Pavlov, 1927a), second-order conditioning has been demonstrated in various vertebrate and invertebrate models (Bitterman et al., 1983; Brembs and Heisenberg, 2001; Hawkins et al., 1998; Mizunami et al., 2009; Tabone and de Belle, 2011; Takeda, 1961). Furthermore, second-order conditioning is thought to extend the applicability of Pavlovian conditioning as an account of behaviors including observational learning (Avarguès-Weber and Chittka, 2014b; Worden and Papaj, 2005b). Additionally, second-order conditioning has also served as a historically important tool for behavioral psychologists to study associative learning by giving them ample options to use virtually any stimulus as a reinforcer (Rescorla, 1980).

One prominent feature that characterizes second-order memory is its transiency, as originally noted by Pavlov and confirmed by other studies using various animal models. That is, the effectiveness of second-order conditioning usually reaches an asymptote after a small number of trials and begins to decline with further training (Gewirtz and Davis, 2000a; Pavlov, 1927b). This decline may be related to the fact that reward is constantly omitted during second-order conditioning. Another important feature of second-order conditioning recognized by behavioral psychologists is that it does not form a tight association between the stimulus and the specific response elicited by the reinforcer, which is typically observed in first-order conditioning (Gewirtz and Davis, 2000b; Pavlov,

1927c). In other words, second-order learning seems to be based on general valence, rather than specific features, of reinforcers. These differences between first- and second-order memories raise important mechanistic questions: What is the circuit origin of those different memory features? Are they different because those two memories are stored in separate circuits that support distinct types of memories? If so, how do the two circuits interact when one memory instructs the other? Answering these questions requires precise mapping of second-order memory circuits.

In rodents, basolateral amygdala and dopaminergic neurons (DANs) play critical roles in second-order learning (Gewirtz and Davis, 1997; Maes et al., 2020a). After first-order association, DANs in the ventral tegmental area acquire enhanced responses at the onset of the cue that predicts upcoming reward after conditioning (Schultz, 1998). A recent study used optogenetic silencing to demonstrate that such cue-evoked dopamine transients are essential for second-order conditioning (Maes et al., 2020b). Whereas DANs consist of functionally diverse populations of neurons, each of which contributing to distinct types of learning (Roeper, 2013; Watabe-Uchida and Uchida, 2018), how these different DAN subtypes interact during second-order conditioning is completely unstudied.

The *Drosophila* mushroom body (MB), a dopamine-rich center for associative learning in insect brains, provides a tractable system to study the interaction between heterogeneous dopamine subsystems. *Drosophila* can perform second-order learning using olfactory or visual cues with punishment (Brembs and Heisenberg, 2001; Tabone and de Belle, 2011), although the underlying circuit mechanisms have not been examined. Decades of studies have revealed the anatomical and functional architecture of the MB circuit (Figure 1A). Along the parallel axonal fibers of Kenyon cells (KCs), DANs and MB output neurons (MBONs) form 16 matched compartments (Aso et al., 2014; Li et al., 2020; Tanaka et al., 2008), which serve as units of associative learning. Reward and punishment activate distinct subsets of 20 types of DANs (Berry et al., 2015; Burke et al., 2012; Kirkhart

and Scott, 2015; Lewis et al., 2015; Lin et al., 2014; Liu et al., 2012; Riemensperger et al., 2005; Siju et al., 2020). Individual DANs write and update memories in each compartment with cell-type-specific dynamics by modulating synaptic connection between KCs and MBONs (Aso and Rubin, 2016; Aso et al., 2012; Hige et al., 2015; Huetteroth et al., 2015; Vrontou et al., 2021; Yamagata et al., 2015). Outside the MB, MBON axons project to regions where DAN dendrites arborize; this provides an anatomical pathway for feedback of memory-based information onto DANs, a potential substrate for higher-order conditioning. Indeed, early studies showed that DANs in the MB dynamically change odor responses after olfactory conditioning (Riemensperger et al., 2005). Furthermore, the recently completed EM connectome (Scheffer et al., 2020) revealed the full wiring diagram of the MB, including intricate connections from MBONs to the DANs. In both larval and adult *Drosophila*, large fractions of synaptic inputs to the MB's DANs originate from the MB itself (Eschbach et al., 2020; Li et al., 2020). Thus it is plausible that induction of synaptic plasticity in one compartment, in turn, affects how a learned stimulus activates DANs and becomes a secondary reinforcer. However, understanding the flow of information across compartments that underlies second-order conditioning is a challenging task, given that thousands of neurons are connected with DANs and MBONs.

Here, by exploiting connectomic data, we identify a key circuit that underlies second-order conditioning. We first establish a protocol for robust olfactory second-order conditioning with sugar reward. In contrast to stable odor-sugar first-order memory, second-order memory decayed within a day and was highly susceptible to extinction. We next show that memory in $\alpha 1$, the compartment responsible for long-lasting appetitive memory (Ichinose et al., 2015; Yamagata et al., 2015), is most potent to promote second-order memory. The second-order memory instructed by $\alpha 1$ was transient during the training phase and extinction trials. Subsequent EM connectome and functional analysis identify a prominent cholinergic interneuron SMP108 that 1) forms an excitatory pathway

from MBON-α1 to DANs in other compartments, 2) acquires an enhanced response to the reward-predicting odor, 3) can promote release of dopamine in multiple compartments, 4) is required for second-order conditioning, and 5) induces memory with fast and transient dynamics. Our study reveals in unprecedented detail circuit mechanisms of second-order conditioning. These mechanisms can explain the different properties of first- and second-order memories. They also provide a concrete example of how hierarchical interaction between dopamine subsystems contributes to a complex form of learning.

Results

Identification of MB compartments that instruct second-order conditioning

As a prerequisite for mapping the underlying neuronal circuits and detailed characterization of memory properties, we established a robust protocol for appetitive second-order conditioning (see Methods for our rationale for the selection of odors and other parameters; Figure 1-figure supplement 1 and 2). Flies were first trained to associate stimulus one (S1) odor with sugar and consolidated that memory for one-day (Figure 1-figure supplement 2A). During second-order conditioning, 20 seconds of one S2 odor (S2+) was immediately followed by 10 seconds of the S1 odor, whereas another S2 odor (S2-) was presented alone in a circular olfactory arena (Figure 1B). After five training sessions, flies increased their preference to the S2+ odor over the S2- odor when first-order conditioning was long enough (i.e. 5min; Figure 1C). This preference for the S2+ odor was not due to sensory preconditioning, another form of higher-order conditioning in which S2-S1 pairing was done *before* pairing S1-sugar (Figure 1-figure supplement 2B).

To identify circuit elements that might be particularly important for second-order conditioning, we examined whether first-order memory in certain MB compartments is more potent for instructing second-order conditioning than others. Flies were first trained by pairing the S1 odor with optogenetic activation of specific DANs with CsChrimson

147 instead of sugar to induce memory in a specific set of compartments (see below for
148 measurement of dopamine release). Then, the compartment-specific memory of the S1
149 odor was tested for its power as a reinforcer in second-order conditioning. Among four
150 sets of DAN cell types that can induce first-order appetitive memory (Figure 1-figure
151 supplement 2C), two sets — PAM-α1 and a combination of PAM-γ5 and β′2a — could
152 induce significant second-order memory compared to the genetic control (Figure 1D).
153 Similar to first-order conditioning, stimulus timing was an important factor for successful
154 second-order conditioning (i.e. S2+ must precede S1; Figure 1-figure supplement 2D).
155 PAM-α1 is known to be essential for learning nutritional value and is required for long-term
156 appetitive memory (Yamagata et al., 2015), whereas memory induced by combinatorial
157 activation of PAM-γ5 and PAM-β′2a is short-lasting (Aso and Rubin, 2016). As expected
158 from those different stabilities of the first-order memory, memory in PAM-α1 but not PAM-
159 γ5/β′2a could instruct second-order conditioning one day after the first-order conditioning
160 (Figure 1D). Consistent with the outcome of this optogenetic experiment, blocking of
161 synaptic transmission from PAM-α1 DANs with Tetanus Toxin (TNT) light chain abolished
162 second-order memory when assayed one day after odor-sugar conditioning (Figure 1E).
163 These results suggest α1 as the primary candidate compartment to mediate first-order
164 memory and instruct second-order conditioning with supplemental contribution by γ5/β′2a
165 compartments.

166 First-order memory in the α1 compartment and its derived second-order memory
167 exhibited marked differences in dynamics of formation and update. The first-order memory
168 steadily increased during nine training sessions, whereas second-order memory peaked
169 at the fifth training and declined subsequently (Figure 1F). This transiency of learning was
170 not observed when DAN activation was not omitted during second-order conditioning
171 (Figure 1F). Also, this transiency of second-order memory was not due to extinction of
172 first-order memory, because flies showed strong preference to S1 even after nine times

presentations of S2-S1 without DAN activation (Figure 1G). We also found that second-order memory was more rapidly extinguished than first-order memory (Figure 1H). Second-order memory after odor-sugar conditioning was also susceptible to extinction and did not last for one day (Figure1-figure supplements 2E and F). These results indicate that the transient and unstable nature of second-order memory observed across animal phyla also applies to *Drosophila*.

Memory in α1 can instruct secondary plasticity across compartments

Memories and plasticity induced in different MB compartments differ in their properties including retention, induction threshold and resistance to extinction (Aso and Rubin, 2016; Aso et al., 2012; Hige et al., 2015; Huetteroth et al., 2015; Jacob and Waddell, 2020; Pai et al., 2013; Plaçais et al., 2013; Vrontou et al., 2021; Yamagata et al., 2015). The markedly distinct memory dynamics between first- and second-order memories noted above prompted us to hypothesize that those memories are formed in different MB compartments. For aversive memory, transient inactivation of MBON-γ1pedc (a.k.a MB-MVP2), which mimics the effect of synaptic depression caused by aversive learning, can serve as reinforcement (König et al., 2019; Ueoka et al., 2017). Thus, if our hypothesis is correct, and if the α1 compartment indeed is potent for instructing second-order conditioning, then local induction of synaptic plasticity in α1 should drive secondary plasticity in other compartments during second-order conditioning. Since PAM-γ5 and β′2a can induce robust appetitive memory that is short-lasting and susceptible to extinction (Figure 1-figure supplement 2C) (Aso and Rubin, 2016), we reasoned that second-order memory may involve compartments targeted by these DANs. To test this idea, we first generated a split-LexA driver to express ChrimsonR selectively in PAM-α1. We then labeled either MBON-α1 or MBON-γ5β′2a by split-GAL4 lines to make whole-cell recordings from them (Figures 2A and Figure 2 -figure supplement 1A). In MBON-α1, we

found that pairing an odor and DAN activation leads to reduced spiking responses to that odor as in other MB compartments examined in previous studies (Figure 2-figure supplement 1) (Berry et al., 2018; Handler et al., 2019; Hige et al., 2015; Owald and Waddell, 2015; Séjourné et al., 2011; Vrontou et al., 2021). MBON-γ5β′2a was, on the other hand, a non-spiking neuron which did not elicit any odor- or current-evoked action potentials. We therefore focused on subthreshold responses. After a single round of second-order conditioning, MBON-γ5β′2a showed reduced responses to the S2+ odor, while responses to S2- did not change even after five repetitions of conditioning (Figure 2B and C). Repeated presentation of S2 odors without S1 did not cause a reduction of odor responses (Figure 2D and E). These results indicate that the α1 compartment can instruct second-order conditioning in the γ5/β′2a and potentially other compartments.

Candidate interneurons to mediate instruction signals for second-order conditioning

We next set out to identify the neuronal pathway responsible for the induction of second-order plasticity. MBON-α1 is the sole output pathway from the α1 compartment and is, like other reward memory compartment MBONs, glutamatergic, which means that they are likely inhibitory (Liu and Wilson, 2013). Upon induction of plasticity, MBON-α1's responses to learned odor will be depressed (Figure 2-figure supplement 1). Therefore, learned odor responses in the downstream circuits of the MBON-α1, which are predicted to be disinhibited after first-order conditioning, could feed DANs in other compartments with necessary excitatory drive for second-order conditioning, provided that there are such connections. However, α1 appears to be an exceptionally isolated compartment. MBON-α1 is the only MBON that does not send output to DANs innervating other compartments; rather it only directly connects with the DAN that innervates the same compartment, PAM-α1 (Figure 3-figure supplement 1A)(Li et al., 2020). Similarly, MBON-α1 shows very limited

connections to DANs innervating other compartments that are mediated by a single interneuron (one-hop pathways; Li et al., 2020; Figure 3-figure supplement 1B). This led us to explore pathways with two interneurons between MBON-α1 and DANs (two-hop pathways).

To explore pathways with interneurons between MBON-α1 and DANs, we queried the hemibrain EM connectome database (Li et al., 2020; Scheffer et al., 2020). We then used a pre-trained machine learning algorithm to predict the most likely neurotransmitters used by the connected neurons (Eckstein et al., 2020). Supplementary File 1 summarizes the full connection matrix, neurotransmitter predictions for the 396 major interneuron cell types with at least 100 total synapses with MBONs and DANs. In this way (see Methods for detail), we identified prominent cholinergic two-hop pathways from MBON-α1 to multiple reward-DANs including PAM-γ5, γ4, β′2a, β′2m, β′2p that were mediated by the interneurons SMP353/354 and SMP108 (Figure 3A). SMP108 also synapses onto all three cholinergic interneurons (SMP177, LHPV5e1, LHPV10d1) in the second layer of the two-hop pathways, providing additional excitatory drive to PAM DANs (Figure 3B). Intriguingly, SMP108 also appeared as an outstanding cell type to receive direct inputs from MBON-γ5β′2a and output to DANs (Figure 3C). As discussed above, we identified the γ5/β′2a as additional compartments that, like α1, can instruct second-order memory. Taken together, the circuit centered at SMP108 appears to be a prominent candidate that converts first-order plasticity in both α1 and γ5β′2a compartments to excitatory drive to DANs.

Identification of SMP108 and its associated circuits allowed us to construct a few testable hypotheses regarding the circuit mechanisms of second-order conditioning. First, SMP108's response to the reward-predicting S1 odor should be potentiated after first-order conditioning. Second, activation of SMP108 should trigger dopamine release in the MB compartments involved in appetitive memory. Third, the output of SMP108 should be required for second-order memory. Fourth, memory induced by the SMP108 pathway

should recapitulate the transient and unstable nature of second-order memory. To experimentally test those hypotheses, we generated split-GAL4 drivers for SMP108 (SS67221 and SS45234; Figures 3D-F). Using these drivers, we confirmed that axonal terminals of SMP108 are immunoreactive to choline acetyltransferase (Figure 3E), which is consistent with the fact that 2,416 out of 2,753 presynaptic sites of SMP108 are predicted to be cholinergic in the hemibrain data (Supplementary File 1).

SMP108 acquires enhanced response to reward-predicting odor

First, we examined the change in SMP108's odor responses after pairing of an odor and optogenetic activation of PAM-cluster DANs, which can induce appetitive memory. As expected from the converging inputs from multiple lateral horn cell types (Supplementary File 1), SMP108 showed robust spiking responses to odors. After pairing, responses to the paired odor were selectively potentiated (Figure 4). Furthermore, reversal pairing de-potentiated the previously paired odor. Thus, SMP108 is capable of acquiring enhanced responses to S1 after first-order conditioning and flexibly tracking updates of odor-reward associations.

SMP108 evokes dopamine release in appetitive memory compartments

Next, we directly measured the pattern of dopamine release evoked by optogenetic activation of SMP108, its upstream neurons (SMP353 and SMP354), or DANs using a recently developed dopamine indicator DA2m (Sun et al., 2020). With direct stimulation of DANs, release of dopamine was largely restricted to the compartment(s) innervated by Chrimson-expressing DANs (Figure 5-figure supplement1). Consistent with EM connectivity, activation of SMP108 or SMP353/354 evoked dopamine release in the reward memory compartments β′2, γ4 and γ5 compartments (Figure 5). SMP108 activation also evoked small dopamine release in β1 and β2, presumably via indirect

277 connections, but not in α1. Notably, we observed that the dopamine signal in γ2, which is
278 tuned to punitive stimuli, was significantly reduced after SMP108 activation (Figure 5-
279 figure supplement 1C). Other DANs for aversive memories such as PAM-γ3, PPL1-
280 γ1pedc, and PPL1-α3 showed very weak response, if any. Thus, activation of SMP108
281 triggers dopamine release selectively in multiple reward memory compartments.
282
283 **SMP108 is required for second-order conditioning**
284 As expected from above results, we found that blocking neurotransmission of SMP108 by
285 expression of TNT using two different split-GAL4 drivers impaired second-order
286 conditioning compared to genetic controls (Figure 6A). We were unable to block SMP108
287 only during the second-order conditioning using the thermogenic effector shibire^{ts1}
288 because flies with control genotype rapidly extinguished the first-order memory and failed
289 to perform second-order conditioning at the 32℃ restrictive temperature (data not shown).
290 Nonetheless, blocking SMP108 with TNT did not impair the first-order memory with 2min
291 or 1-day retention (Figure 6B), indicating that flies with blocked SMP108 were fully capable
292 of smelling odors, tasting sugar, and forming, consolidating, and retrieving the first-order
293 appetitive memory.
294 To further assess the potential contribution of SMP108 to appetitive memory
295 retrieval, we tested whether activation of SMP108 triggers any relevant behavior. Flies
296 steer to an upwind orientation in the presence of reward-predicting odors and food-related
297 odors like vinegar (Álvarez-Salvado et al., 2018; Borst and Heisenberg, 1982; Handler et
298 al., 2019). Upon optogenetic stimulation of SMP108 with CsChrimson, flies indeed
299 changed their mean orientation and walked upwind in the same circular arena used in the
300 olfactory conditioning experiments described above (Figure 6-figure supplement 1A).
301 However, we did not observe any impairment of upwind steering in response to the sugar-
302 associated odor in SMP108-blocked flies (Figure 6-figure supplement 1B), suggesting the

existence of redundant circuits that trigger memory-based upwind steering. Thus, SMP108 could contribute to retrieval of reward memory for guiding actions, but its requirement is limited to second-order conditioning. Taken together, these results indicate that SMP108, which we identified as a prominent anatomical hub for the feedforward circuit between reward memory compartments, indeed plays a key role in second-order conditioning by triggering dopamine signals in response to the reward-predicting cue.

SMP108 pathway induces transient memory

Based on the results so far, we propose a teacher-student compartment model that explains the induction mechanism of second-order memory and its distinct dynamics from first-order memory (Figure 7A). In this model, local plasticity induced in a stable memory compartment (i.e. α1) during first-order conditioning function as a reinforcer to induce secondary plasticity in other transient memory compartments through interneurons (i.e. SMP108) that connect those memory compartments. Thus, this model predicts that target compartments of SMP108 pathway collectively express transient memory dynamics that recapitulates unstable nature of second-order memory (Figures 1F, 1H, Figure 1-figure supplements 2E-F).

To test this prediction, we next examined the dynamics of memory induced by the SMP108 pathway in detail and compared them to those induced by direct stimulation of PAM-α1 and other DAN types using CsChrimson (Figures 7B and Figure 7-figure supplement 1). The protocol started by assessing naïve odor preference that was designed to be canceled by reciprocal experiments. Then flies were sequentially trained five times by 10s, 30s, 60s, 60s and 60s periods of odor presentation paired with LED activation, and then another odor presented without LED activation (training phase). Memory was tested by giving a choice between odors after each training. After the fifth training, memory was tested 12 times without pairing with LED activation (extinction

329 phase). Then flies were trained with a reversal protocol 5 times and tested 12 times
330 (reversal phase). After one more round of reversal phase (re-reversal), flies were exposed
331 to LED activation without odor to test the susceptibility of memory to non-contingent
332 activation of DANs, a protocol that is known to erase memory (Berry et al., 2012; Plaçais
333 et al., 2012). These experiments revealed that memories induced by SMP108 or its
334 upstream SMP353/354 differ in several ways from the memory induced by activation of
335 PAM-α1 (Figure 7C-F). First, SMP108 and SMP353/354 can induce memory more rapidly
336 than PAM-α1 (Figure 7C). Second, memories formed by SMP108 and SMP353/354
337 declined during later training sessions and during the extinction phase, whereas memory
338 formed by PMA-α1 remained high (Figure 7D and E). Third, memory formed by PAM-α1
339 was resistant to DAN activation, but memories formed by SMP108 and SMP353/354 were
340 decreased (Figure 7F). Such transient learning and fast extinction are reminiscent of
341 second-order conditioning (Figures 1F, 1H, Figure 1-figure supplements 2E-F). In contrast
342 to the activation of CsChrimson in PAM-α1, drivers that target CsChrimson to SMP108's
343 downstream DANs exhibited memory dynamics similar to those observed when
344 CsChrimson is activated in SMP108 or SMP353/354. For instance, MB032B and MB213B
345 split-GAL4 that target CsChrimson in β′2m and β1/β2, respectively, induced transient
346 memories (Figure 7E). Consistent with this, fitting the memory dynamics formed by
347 SMP108 with a linear sum of direct DAN activation data indicated an overweight of
348 MB032B (β′2m), MB213B (β1/β2) and MB312C (γ4), and zero weight for MB043C (α1)
349 (Figure 7G). However, the high memory score of SMP108 activation after the first 10s
350 training was fitted poorly, indicating that combinatorial activation of DANs and/or
351 suppression of DANs innervating γ2 (Figure 5-figure supplement 1C) might have a
352 synergistic effect on memory formation. These experiments highlight the distinct memory
353 properties exhibited by upstream and downstream partners of SMP108, and might help

354 explain the circuit mechanisms underlying the difference between first- and second-order
355 memories.
356
357 **Discussion**

358 In this study, we used the *Drosophila* mushroom body as a model system to examine how
359 multiple dopamine-driven memory circuits interact to enable second-order conditioning.
360 Although second-order conditioning has been demonstrated behaviorally in many species,
361 there is little circuit-level knowledge to provide mechanistic insight. By developing a robust
362 appetitive second-order conditioning protocol and utilizing the EM connectome map in
363 *Drosophila*, we uncovered neural circuit mechanisms that define dynamics and learning
364 rules of second-order conditioning.
365
366 **Origins of the unique learning rules of second-order conditioning**
367 Our optimization of the second-order conditioning protocol in flies revealed important
368 properties of second-order memory and enabled detailed circuit interrogation. Flies formed
369 second-order memory only when the first-order S1 odor predicted a strong reward (Figure
370 1C) and only if the second-order S2 odor preceded the S1 odor (Figure 1-figure supplement
371 2D). With additional training sessions, second-order memory could become as robust as
372 the first-order memory, but the continual omission of the expected reward during training
373 and extinction trials tended to reduce second-order memory (Figures 1F and 1H). The
374 retention of second-order memory was also shorter than first-order memory (Figure 1-figure
375 supplement 2E). Remarkably, all the dynamics and learning rules we found in *Drosophila*
376 for second-order conditioning are well-conserved across animal phyla (Gewirtz and Davis,
377 2000b; Pavlov, 1927c; Rescorla, 1980). Our study indicates that, in flies, at least some of
378 these phenomena can be accounted for by the teacher-student model of the MB circuit,

379 which hypothesizes distinct dynamics of plasticity in individual compartments and
380 hierarchical interactions between compartments. Namely, a compartment with a slow
381 learning rate instructs compartment(s) with transient memory dynamics.

382 Requirement of long first-order training for successful formation of second-order
383 memory (Figure 1C and Figure 1-figure supplement 2A) can be explained by the properties
384 of the α1, which we identified as the teacher compartment. The DANs in α1 respond to sugar
385 relatively weakly compared to other DANs in the β′2, β2, γ4, γ5 compartments (Siju et al.,
386 2020). Also the α1 compartment exhibited the slowest learning rate of all compartments
387 even with optogenetic stimulation of DANs that efficiently release dopamine (Figure 5-figure
388 supplement 1 and Figure 7C). Once established, however, memory in the α1 is highly
389 resistant to extinction (Figure 1-figure supplement 2C and Figure 7D), which is likely critical
390 for forming second-order conditioning without compromising first-order memory. These
391 considerations emphasize the eligibility of the α1 compartment as a teaching compartment
392 among all reward-memory compartments. On the other hand, transient and unstable nature
393 of second-order memory can be ascribed to collective properties of student compartments
394 (Figure 7). Future studies are required to identify intrinsic molecular factors and microcircuit
395 elements responsible for distinct dynamics of teacher and student compartments.
396
397 **Implications to the higher-order functions of heterogeneous dopamine subsystems**
398 Our study identified a role of hierarchical interaction between dopamine-based memory
399 subsystems. Importantly, heterogeneous populations of DANs are also found in vertebrate
400 species, and they are involved in distinct types of learning. Studies using visual conditioning
401 in monkeys found that distinct types of DANs projecting to the head or tail regions of the
402 caudate nucleus change their response to reward-predicting cues with very different
403 dynamics (Kim et al., 2014, 2015). A recent study in rodents indicated that subsets of DANs
404 have diverse learning rates to compute positive and negative reward prediction errors to

enable distributional reinforcement learning (Dabney et al., 2020). Cue-evoked dopamine transients at the onset of reward-predicting cues are required for second-order conditioning in rodents (Maes et al., 2020a). Such dopamine transients could be derived from memory encoded by the same DAN, other type(s) of DANs, or both, depending on the architecture of feedback circuits. Given the conserved nature of second-order memory transiency across animal phyla, future studies in vertebrate models may also reveal a hierarchical interaction between dopamine cell types with fast and slow dynamics in second-order conditioning.

Second-order conditioning is merely one example of learning that depends on higher-order connections between dopamine-dependent memory subsystems. In fact, in flies, feedback and feedforward connections between MBONs and DANs or lateral connections between MBONs are implicated in extinction of aversive and appetitive memory as well as consolidation of memories (Felsenberg et al., 2017, 2018; McCurdy et al., 2021). The EM connectome map, along with computational modeling (Gkanias et al.; Jiang and Litwin-Kumar), will guide further investigation of intercompartmental interactions. For instance, we identified one outlier cell type of GABAergic interneuron LHCENT3 that receives inputs from glutamatergic MBON-γ5β′2a and outputs to reward DANs (Figure 3C). This cell type may serve as the substrate for subtraction of expected reward in the computation of reward prediction error, as GABAergic neurons in VTA do in vertebrate brains (Starkweather and Uchida, 2021). Although the majority of circuit-level research has focused on rather simple forms of learning that involve primary reinforcers, animals have abundant opportunities to shape their behaviors through indirect learning that depends on existing memory. We expect that network motifs similar to what we identified here contribute to various forms of such complex learning. We expect that future modeling studies constrained by the EM connectome and large scale behavioral and neural activity data will lead to a comprehensive understanding of mushroom body's contributions to these computations.

Contents of second-order conditioning

Understanding what is learned is a fundamental challenge in studies of associative learning. There are many possible structures of associations that would allow animals to perform second-order conditioning tasks. Our finding of the cross-compartmental nature of second-order conditioning makes it unlikely that flies associate S2 with a *specific* type of reward used as US, because individual MB compartments are tuned to different kinds of rewards or reward responses. That is, while DANs in the teacher compartment α1 are essential for nutritional value learning (Yamagata et al., 2015), those in the student compartments γ4 and β′2 respond to water in thirsty flies (Lin et al., 2014). DANs in γ4, γ5 and β′2 also represent vinegar and activity of DANs in γ4 correlates with upwind steering (Lewis et al., 2015; Zolin et al., 2021). DANs in β′2a also respond to a punishment-predicting odor when punishment is omitted (McCurdy et al., 2021). Thus, based on our circuit mapping and the known functions of the relevant circuits, we propose that S2 is associated with positive valence that was originally associated with S1 but generalized to broader types of rewards. This view is consistent with the fact that second-order conditioning is typically insensitive to subsequent reduction of the value of the US (i.e. devaluation), which suggests that an association is formed between S2 and the original valence of the US rather than the US itself (Rescorla, 1980). Studies in rodents demonstrated that S1 and S2 with different sensory modalities can elicit distinct conditioned responses (CRs), supporting the idea that S2 is not associated with the specific CR elicited by S1 (Holland, 1977; Kim et al., 1996). Notably, a broadening of the category of expected rewards in second-order conditioning has been suggested by a study in pigeons (Stanhope, 1992), where differential CRs to qualitatively distinct USs (i.e. food and water) were observed for S1 but not for S2. Thus, our circuit underpinning of second-order conditioning provides a concrete neuronal substrate for behavioral and psychological phenomena that have been described for decades.

Materials and Methods

Fly strains

Drosophila melanogaster strains were reared at 22C and 60% humidity on standard cornmeal food in 12:12 hour light:dark cycle. 4-10 days of adult females were used 2-4 days after sorting them on the Peltier cold plate. For flies expressing Chrimson (Klapoetke et al., 2014) the food was supplemented with retinal (0.2 mM all-trans-retinal prior to eclosion and then 0.4 mM). Driver and effector lines are listed in the key resource table (Supplementary File 2) and genotypes used by each figure are listed below. The new collection of split-GAL4 drivers was designed based on confocal image databases (http://flweb.janelia.org) (Jenett et al., 2012), and screening expression patterns of p65ADZp and ZpGAL4DBD combinations as described previously (Aso et al., 2014; Pfeiffer et al., 2010). Confocal stacks of new split-GAL4 driver lines used in this study are available at http://www.janelia.org/split-gal4.

Detailed fly genotypes used by figures

Figure	Genotype
Figure1 C, Figure 1-figure supplement 1, 2A,B,E,F	*Canton S*
Figure 1D, Figure 1-figure supplement 2C	*w/w, 20xUAS-CsChrimson-mVenus attP18;;+/MB043C-split-GAL4* *w/w, 20xUAS-CsChrimson-mVenus attP18;+/MB213B-split-GAL4* *w/w, 20xUAS-CsChrimson-mVenus attP18;;+/MB312C-split-GAL4* *w/w, 20xUAS-CsChrimson-mVenus attP18;MB109B/MB315C-split-GAL4* *w/w, 20xUAS-CsChrimson-mVenus attP18;MB109B/ Empty-split-GAL4*
Figure 1E-H, Figure 1-figure supplement 2D	*w/+;MB043C/+* *w/+;MB043C/UAS-TNT (II)* *w/+;Empty-split-GAL4/TNT (II)*
Figure 1-figure supplement 2D-G	*w/w, 20xUAS-CsChrimson-mVenus attP18;+/+;+/MB043C-split-GAL4*
Figure 2	*w/w,13XLexAop2-IVS-ChrimsonR-mVenus-p10 attP18, 20XUAS-syn21 mScarlet-opt-p10 su(Hw)attp8; SS01308-split-GAL4/MB043-split-LexA*
Figure 2-figure supplement 1	*w/w,13XLexAop2-IVS-ChrimsonR-mVenus-p10 attP18, 20XUAS-syn21 mScarlet-opt-p10 su(Hw)attp8; MB319C-split-GAL4/MB043-split-LexA*
Figure 3E	*w/w, pJFRC200-10xUAS-IVS-myr::smGFP-HA in attP18; pJFRC225-5xUAS-IVS-myr::smGFP-FLAG in VK00005/SS67221-split-GAL4*
Figure 3F	*pBPhsFlp2::PEST in attP3;; pJFRC201-10XUAS-FRT>STOP>FRT-myr::smGFP-HA in VK0005, pJFRC240-10XUAS-FRT>STOP>FRT-myr::smGFP-V5-THS-10XUAS-FRT>STOP>FRT-myr::smGFP-FLAG in su(Hw)attP1/SS67221-split-GAL4*
Figure 4	*13XLexAop2 IVS p10 ChrimsonR mVenus trafficked in attP18/+; 58E02-LexAp65 in attP40/ VT026646-p65ADZp in attP40 (ss45234-split); pJFRC28-10XUAS-IVS-GFP-p10 in su(Hw)attP1 / VT029309-ZpGdbd in attP2 (ss45234-split)*
Figure 5, Figure 5-figure supplement 1	*w/w, 10XUAS-Chrimson88-tdTomato attP18; 13F02-LexAp65 attP40; LexAop2-DA2m VK00005/MB043C-split-GAL4* *w/w, 10XUAS-Chrimson88-tdTomato attP18; 13F02-LexAp65 attP40; LexAop2-DA2m VK00005/MB213B-split-GAL4* *w/w, 10XUAS-Chrimson88-tdTomato attP18; 13F02-LexAp65 attP40; LexAop2-DA2m VK00005/MB032B-split-GAL4* *w/w, 10XUAS-Chrimson88-tdTomato attP18; 13F02-LexAp65 attP40; LexAop2-DA2m VK00005/MB109B-split-GAL4* *w/w, 10XUAS-Chrimson88-tdTomato attP18; 13F02-LexAp65 attP40; LexAop2-DA2m VK00005/MB315C-split-GAL4* *w/w, 10XUAS-Chrimson88-tdTomato attP18; 13F02-LexAp65 attP40; LexAop2-DA2m VK00005/MB312C-split-GAL4* *w/w, 10XUAS-Chrimson88-tdTomato attP18; 13F02-LexAp65 attP40; LexAop2-DA2m VK00005/SS33917-split-GAL4* *w/w, 10XUAS-Chrimson88-tdTomato attP18; 13F02-LexAp65 attP40; LexAop2-DA2m VK00005/SS67221-split-GAL4*
Figure 6	*w/+;SS67221/+* *w/+; SS67221/UAS-TNT (II)* *w/+;SS45234/+* *w/+; SS45234/UAS-TNT (II)* *w/+;Empty-split-GAL4/TNT (II)SS67221/TNT*
Figure 6-figure supplement 1A	*w/w, 20xUAS-CsChrimson-mVenus attP18;+/ Empty-split-GAL4* *w/w, 20xUAS-CsChrimson-mVenus attP18;+/SS67221-split-GAL4*
Figure 6-figure supplement 1B	*w/+;SS67221/+* *w/+; SS67221/UAS-TNT (II)* *w/+;Empty-split-GAL4/TNT (II)SS67221/TNT*
Figure 7, Figure 7-figure supplement 1	*w/w, 20xUAS-CsChrimson-mVenus attP18;+/+;+/MB043C-split-GAL4* *w/w, 20xUAS-CsChrimson-mVenus attP18;+/SS33917-split-GAL4* *w/w, 20xUAS-CsChrimson-mVenus attP18;+/SS67221-split-GAL4* *w/w, 20xUAS-CsChrimson-mVenus attP18;+/MB032B-split-GAL4* *w/w, 20xUAS-CsChrimson-mVenus attP18;+/MB109B-split-GAL4* *w/w, 20xUAS-CsChrimson-mVenus attP18;+/+;+/MB315C-split-GAL4* *w/w, 20xUAS-CsChrimson-mVenus attP18;+/MB312C-split-GAL4* *w/w, 20xUAS-CsChrimson-mVenus attP18;+/MB213B-split-GAL4*

Olfactory conditioning

Olfactory conditioning was performed as previously described (Aso et al., 2016). Groups of approximately 20 females of 4–10 d post-eclosion were trained and tested using the modified four-field olfactory arena (Aso and Rubin, 2016; Pettersson, 1970) equipped with the 627nm LED board (34.9 μW/mm2 at the position of the flies) and odor mixers. The flow rate of input air from each of the four arms was maintained at 100 mL/min throughout the experiments by mass-flow controllers, and air was pulled from the central hole at 400 mL/min. Odors were delivered to the arena by switching the direction of airflow to the tubes containing diluted odors using solenoid valves. The odors were diluted in paraffin oil: 3-octanol (OCT 1:1000), 4-methylcyclohexanol (MCH; 1:750), Pentyl acetate (PA: 1:10000) and ethyl lactate (EL: 1:10000). Sugar conditioning was performed by using tubes with sucrose absorbed Whatman 3 MM paper as previously described (Krashes and Waddell, 2008; Liu et al., 2012). Before conditioning, flies were starved for 40-48 hour on 1% agar. Videography was performed at 30 frames per second and analyzed using Fiji. For experiments with one day retention, flies were kept in agar vials at 21C after first-order conditioning. For testing olfactory memories, distribution of flies in four quadrants were measured for 60 s. The performance index (PI) is defined as a mean of [(number of flies in the two diagonal quadrants filled the one odor) - (number of flies in other two quadrants filled with another odor or air)]/(total number of flies) during final 30 s of 60 s test period. The average PI of reciprocal experiments is shown in figures to cancel out potential position bias and innate odor preference.

Optimization of second-order conditioning

To establish a training protocol for robust olfactory second-order conditioning in *Drosophila*, we first characterized how innate preference for an odor (when compared with pure air) changes over multiple trials using the four-armed olfactory arena (Figure-figure supplement 1)(Aso and Rubin, 2016; Pettersson, 1970). We previously chose concentrations of two conventional odors, 4-methylcyclohexanol (MCH) and 3-octanol (OCT), so that naïve fed flies show behavioral responses to each odor at a similar level, minimizing bias between them (Tully and Quinn, 1985). At the same concentration, starved flies showed slight attraction to the MCH at the first trial, then gradually shifted to aversion in subsequent trials (Figure 1-figure supplement 1). In contrast, both fed and starved flies showed aversion to the OCT, which gradually decreased in subsequent trials. Because the innate aversiveness of OCT may preclude appetitive second-order conditioning, we decided to use MCH as the first conditioned stimulus (S1) throughout this study.

The strength of second-order conditioning tends to be low, compared to that of first-order, but can be enhanced by using an unconditioned stimulus (US) of high intensity and sensory stimuli within the same modality (Helmstetter and Fanselow, 1989; Rescorla and Furrow, 1977). Thus, we examined the effect of increasing conditioning duration. After pairing MCH with sugar for increasing durations (0, 2, 5 min), flies were allowed to consolidate the memory for one day. Then the stability of first-order memory was tested by repeating binary choice between S1 odor and air for 12 times. All trained flies showed attraction to MCH during at least the first five trials (Figure 1-figure supplement 2). One 2-min training was enough to induce appetitive memory (Krashes and Waddell, 2008; Tempel et al., 1983), but longer 5-min training resulted in slightly stronger memories during the first five tests on average. Therefore, we decided to limit the number of second order

conditioning to five times. We used two odorants, pentyl acetate (PA) and ethyl lactate (EL) as the second conditioned stimuli (S2). These odors are known to evoke discrete patterns of activity in Kenyon cells (Campbell et al., 2013) and thought to be easily discriminated against. Innate behavioral responses to these odors were relatively stable over 12 trials (Figure 1-figure supplement 1).

For first-order conditioning, flies learn best when sensory cues precede US or DAN activation (Aso and Rubin, 2016; Tanimoto et al., 2004). Thus, during second-order conditioning, 20 seconds of one S2 odor (S2+) was immediately followed by 10 seconds of the S1 odor, whereas another S2 odor (S2-) was presented alone. Flies failed to form second-order memory when S1 preceded S2+ (Figure 1-figure supplement 2D). PA and EL were S2+ and S2- odors, respectively, in half of a set of reciprocal experiments. The S2+ and S2- odors were swapped in the other half of reciprocal experiments. After five training sessions, unpaired control flies showed weak attraction to S2+, possibly due to innate attractiveness of MCH in starved flies (Figure 1-figure supplement 1). Compared to this basal response, flies preferred the S2+ odor over the S2- odor when first-order conditioning was long enough (i.e. 5min; Figure 1C). This preference for the S2+ odor was not due to stimulus generalization of S1 (MCH) to PA or EL, because such bias is designed to be canceled by our experimental design involving reciprocal experiments. Both immediate and one-day first-order memories were potent to induce second-order memory, but second-order memory did not last for one day (Figure 1-figure supplement 2E).

Response Airflow

For testing airflow directional response, we used the same circular olfactory arena (Figure 6-figure supplement 1), in which air flows from peripheral to a hole at the center. Each fly's distance from center (r_i) was measured and area normalized index (r_i/r_{arena})*(r_i/r_{arena}) was calculated. r_{arena} is the radius of the arena. When flies distribute randomly in the arena, mean r is 1/sqrt(2) and area normalized index is 1/2. To calculate upwind displacement, the mean of arena normalized distance from center at each time point in each movie was subtracted by that at the onset of LED or odor.

Electrophysiology

Fly stocks for electrophysiological experiments were maintained at room temperature on conventional cornmeal-based medium (Archon Scientific). Experimental flies were collected on the day of eclosion, transferred to all-trans-retinal food (5 mM) and kept in the dark for 48-72 hr. For second-order conditioning experiments, flies were starved for 60-72 hr after feeding retinal food.

In vivo whole-cell recordings were performed as previously reported (Hige et al., 2015). The patch pipettes were pulled for a resistance of 4-6MΩ and filled with pipette solution containing (in mM): L-potassium aspartate, 140; HEPES, 10; EGTA, 1.1; $CaCl_2$, 0.1; Mg-ATP, 4; Na-GTP, 0.5 with pH adjusted to 7.3 with KOH (265 mOsm). The preparation was continuously perfused with saline containing (in mM): NaCl, 103; KCl, 3; $CaCl_2$, 1.5; $MgCl_2$, 4; $NaHCO_3$, 26; N-tris(hydroxymethyl) methyl-2-aminoethane-sulfonic acid, 5; NaH_2PO_4, 1; trehalose, 10; glucose, 10 (pH 7.3 when bubbled with 95% O_2 and 5% CO_2, 275 mOsm). For recordings from starved flies, trehalose and glucose were replaced by equimolar sucrose. Whole-cell recordings were made using the Axon MultiClamp 700B amplifier (Molecular Devices). Target cells were visually targeted by fluorescence signal with a 60X water-immersion objective (LUMPlanFI/IR; Olympus) attached to an upright microscope (OpenStand; Prior Scientific). Cells were held at around -60 mV by injecting

hyperpolarizing current, which was typically < 100 pA. Signals were low-pass filtered at 5 kHz and digitized at 10 kHz.

For odor delivery, a previously described custom-designed device was used (Hige et al., 2015). Saturated head space vapors of pure chemicals were air-diluted to 0.5 % (for second-order conditioning) or 2% (for the other experiments) before being presented to flies. Photostimulation was delivered by a high-power LED source (LED4D067; Thorlabs) equipped with 625 nm LED. Light pulses controlled by an LED driver (DC4100; Thorlabs) were presented to the brain at 17 mW/mm^2 through the objective lens.

Data acquisition and analyses were done by custom scripts in MATLAB (MathWorks). Instantaneous spike rates were calculated by convolving spikes with a Gaussian kernel (SD = 50 ms). Subthreshold odor responses and odor-evoked spikes were calculated with the time window of 1.2 s (for 1-s odor presentation) or 20.6 s (for 20-s odor presentation) from odor onset. Spontaneous spikes were subtracted to calculate odor-evoked spikes.

Dopamine imaging

Virgin females of *10XUAS-Chrimson88-tdTomato attP18; R13F02-LexAp65 in attP40;LexAop2-DA2m in VK00005* (Klapoetke et al., 2014; Sun et al., 2020) were crossed with split-GAL4 driver lines, and progenies were reared at 25 ℃ on retinal supplemented (0.2 mM) cornmeal medium that was shielded from light. All experiments were performed on female flies, 3-7 days after eclosion. Brains were dissected in a saline bath (103 mM NaCl, 3 mM KCl, 2 mM CaCl2, 4 mM MgCl2, 26 mM NaHCO3, 1 mM NaH2PO4, 8 mM trehalose, 10 mM glucose, 5 mM TES, bubbled with 95% O2 / 5% CO2). After dissection, the brain was positioned anterior side up on a coverslip in a Sylgard dish submerged in 3 ml saline at 20℃. The sample was imaged with a resonant scanning 2-photon microscope with near-infrared excitation (920 nm, Spectra-Physics, INSIGHT DS DUAL) and a 25× objective (Nikon MRD77225 25XW). The microscope was controlled using ScanImage 2016 (Vidrio Technologies). Images were acquired over a 231 µm × 231 µm x 42 µm volume with a step size at 2 µm. The field of view included 512 × 512 pixel resolution taken at approximately 1.07 Hz frame rate. The excitation power during imaging was 19 mW.

For the photostimulation, the light-gated ion channel CsChrimson was activated with a 660-nm LED (M660L3 Thorlabs) coupled to a digital micromirror device (Texas Instruments DLPC300 Light Crafter) and combined with the imaging path with a FF757-DiO1 dichroic (Semrock). On the emission side, the primary dichroic was Di02-R635 (Semrock), the detection arm dichroic was 565DCXR (Chroma), and the emission filters were FF03-525/50 and FF01-625/90 (Semrock). An imaging session started with a 30 s baseline period, followed by a 1 s stimulation period when 12 µW/mm2 photostimulation light was delivered, and responses were detected over a 30 s post stimulation period. This was repeated for 10 trials. The light intensity was measured using the Thorlabs S170C power sensor.

For quantification of dopamine sensor signals, we used custom python scripts to draw ROIs corresponding to mushroom body compartments on maximum intensity projection over time. Before calculating the change in fluorescence (ΔF), fluorescence from a background ROI was subtracted. The background ROI was drawn in a region with no fluorescence. Baseline fluorescence is the mean fluorescence over a 30 s time period before stimulation started. The ΔF was then divided by baseline to normalize signal (ΔF/F). The mean responses from the 10 trials were calculated for each animal (4-6 samples per driver). Kruskal-Wallis H (KW) test was used for multi-comparison. Post-hoc pairwise comparison was made with the Wilcoxon rank-sum test.

Connectivity analysis

For producing the connectivity data shown in Figures 3 and Figure 3-figure supplement 1, connectivity information was retrieved from neuPrint (neuprint.janelia.org) hosting the "hemibrain" dataset (Scheffer et al., 2020), which is a publicly accessible web site (https://doi.org/10.25378/janelia.12818645.v1). For cell types, we cited cell type assignments reported in Sheffer et al., 2020. Only connections of the cells in the right hemisphere were used due to incomplete connectivity in the left hemisphere (Zheng et al., 2018). Connectivity data was then imported to a software Cytoscape (https://cytoscape.org/) for generating the diagrams before finalizing on Illustrator. The 3D renderings of neurons presented were generated using the visualization tools of NeuTu (Zhao et al., 2018) or VVD viewer (https://github.com/takashi310/VVD_Viewer; (Wan et al., 2012).

Neurotransmitter prediction

The method for neurotransmitter prediction using electron microscopy images and a 3D VGG-style network were described in detail for the FAFB data of a whole fly brain (Eckstein et al., 2020; Zheng et al., 2018). We used the same approach to train the network to classify individual presynaptic sites of FIB-SEM hemibrain data into the same six major neurotransmitters in fly brains as for FAB, i.e.: GABA, glutamate, acetylcholine, serotonin, dopamine and octopamine. Due to the differences in resolution between FAFB and the electron microscopy images used here, we adapted the architecture of the 3D VGG network to be isotropic as follows: We use four downsampling layers with uniform pooling sizes of 2x2x2 on 3D crops centered on synapses with a side-length of 80 voxels. The results for 396 major interneurons are summarized in Supplementary File 1.

Immunohistochemistry

Brains and ventral nerve cord of 4-10 days old female were dissected, fixed and immunolabeled as previously described using the antibodies listed in the Supplementary File 2 Key Resource Table (Aso et al., 2014; Nern et al., 2015). Samples were imaged with confocal microscopes (Zeiss LSM710, LSM780 or LSM880). Inset images in Figure 3E were taken with Airyscan.

Regression analysis of SMP108 memory dynamics

For each strain, the log-probability ratio of reinforced vs. unreinforced stimuli was computed as $R = log(p/(1-p))$, where p is the probability of choosing the reinforced stimulus. To relate the memory dynamics induced by SMP108 to those induced by DANs that it activates, we performed non-negative linear least-squares regression of the log-probability ratio for SMP108 against the ratios for PAM DANs. This reflects an assumption that the combinatorial activation of multiple compartments contributes a behavioral bias that is additive in log-probability ratio.

Statistics

Statistical comparisons were performed on Graphpad Prism or MATLAB using the Kruskal Wallis test followed by Dunn's post-test for multiple comparison, t-tests, or two-way ANOVA followed by Tukey's post hoc multiple comparisons test designated in figure legends.

Data and Code Availability

The confocal images of expression patterns are available online (http://www.janelia.org/split-gal4). Customized MATLAB, Python scripts and data in this paper are available upon request to (asoy@janelia.hhmi.org). A complete construction documentation, CAD files, for the olfactory arena are available through the Janelia TechTransfer office (techtransfer@janelia.hhmi.org) upon request.

Supplemental information

Supplementary File 1 Neurotransmitter prediction and a full connection matrix for MBONs, DANs and 396 interneurons cell types.
Numbers in column B-G are number of presynaptic sites that are predicted to be designated neurotransmitters. EM id in column K is identification number in EM hembrain data. The other columns are the connection matrix. Top raw indicates direction of connections. For instance, 153 in the raw 5 of column M indicate the number of connections from MBON01 to SMP108, while 166 in the raw5 of column BD indicate the number of connections from SMP108 to PAM02. For the cell type consisting of multiple cells, a summed number of connections are shown.

Supplementary File 2 Key Resource Table

Acknowledgments

We thank James Fitzgerald, Sandro Romani, Gerald M. Rubin, Yichun Shuai, Mehrab Modi, Zongwei Chen, Adithya Rjagopalan and members of the Y.A. and T.H. lab for valuable discussion and comments on the manuscript. We thank all the members of Janelia Flylight, fly facility and scientific computing for generation and confocal microscopy images of split-GAL4 drivers. D.Y. was supported by Toyobo Biotechnology Foundation Postdoctoral Fellowship and Japan Society for the Promotion of Science Overseas Research Fellowship. Y.A. was supported by HHMI. T.H. was supported by NIH (R01DC018874), NSF (2034783), BSF (2019026) and UNC Junior Faculty Development Award. A.L.-K. was supported by the Burroughs Wellcome Foundation, the Gatsby Charitable Foundation, the McKnight Endowment Fund, the Simons Collaboration on the Global Brain, NIH award R01EB029858, and NSF award DBI-1707398.

Author contributions

Conceptualization, D.Y., A.L.K., T.H. and Y.A. ; Formal Analysis, D.Y., D.B., L.F., M.S., J.F., A.L.K. and Y.A. ;Investigation, D.Y., D.B., K.H., J.F. and Y.A. ;Writing - Original Draft, D.Y., T.H. and Y.A.; Writing - Review & Editing, D.Y., D.B., L.F., M.S., J.F., A.L.K., T.H. and Y.A.; Supervision, T.H. and Y.A.; Funding Acquisition, A.L.K., T.H. and Y.A.

Competing interests

The authors declare no competing interests.

References

Álvarez-Salvado, E., Licata, A.M., Connor, E.G., McHugh, M.K., King, B.M., Stavropoulos, N., Victor, J.D., Crimaldi, J.P., and Nagel, K.I. (2018). Elementary sensory-motor transformations underlying olfactory navigation in walking fruit-flies. Elife

705 *7*.

706 Aso, Y., and Rubin, G.M. (2016). Dopaminergic neurons write and update memories with
707 cell-type-specific rules. Elife *5*.

708 Aso, Y., Herb, A., Ogueta, M., Siwanowicz, I., Templier, T., Friedrich, A.B., Ito, K.,
709 Scholz, H., and Tanimoto, H. (2012). Three dopamine pathways induce aversive odor
710 memories with different stability. PLoS Genet. *8*, e1002768.

711 Aso, Y., Hattori, D., Yu, Y., Johnston, R.M., Iyer, N.A., Ngo, T.-T.B., Dionne, H., Abbott,
712 L.F., Axel, R., Tanimoto, H., et al. (2014). The neuronal architecture of the mushroom
713 body provides a logic for associative learning. Elife *3*, e04577.

714 Avarguès-Weber, A., and Chittka, L. (2014). Observational conditioning in flower choice
715 copying by bumblebees (Bombus terrestris): influence of observer distance and
716 demonstrator movement. PLoS One 9, e88415.

717 Berry, J.A., Cervantes-Sandoval, I., Nicholas, E.P., and Davis, R.L. (2012). Dopamine is
718 required for learning and forgetting in Drosophila. Neuron *74*, 530–542.

719 Berry, J.A., Cervantes-Sandoval, I., Chakraborty, M., and Davis, R.L. (2015). Sleep
720 Facilitates Memory by Blocking Dopamine Neuron-Mediated Forgetting. Cell *161*, 1656–
721 1667.

722 Berry, J.A., Phan, A., and Davis, R.L. (2018). Dopamine Neurons Mediate Learning and
723 Forgetting through Bidirectional Modulation of a Memory Trace. Cell Rep. *25*, 651–
724 662.e5.

725 Bitterman, M.E., Menzel, R., Fietz, A., and Schäfer, S. (1983). Classical conditioning of
726 proboscis extension in honeybees (Apis mellifera). J. Comp. Psychol. *97*, 107–119.

727 Borst, A., and Heisenberg, M. (1982). Osmotropotaxis inDrosophila melanogaster.
728 Journal of Comparative Physiology ? A *147*, 479–484.

729 Brembs, B., and Heisenberg, M. (2001). Conditioning with compound stimuli in
730 Drosophila melanogaster in the flight simulator. J. Exp. Biol. *204*, 2849–2859.

731 Burke, C.J., Huetteroth, W., Owald, D., Perisse, E., Krashes, M.J., Das, G., Gohl, D.,
732 Silies, M., Certel, S., and Waddell, S. (2012). Layered reward signalling through
733 octopamine and dopamine in Drosophila. Nature *492*, 433–437.

734 Campbell, R.A.A., Honegger, K.S., Qin, H., Li, W., Demir, E., and Turner, G.C. (2013).
735 Imaging a population code for odor identity in the Drosophila mushroom body. J.
736 Neurosci. *33*, 10568–10581.

737 Dabney, W., Kurth-Nelson, Z., Uchida, N., Starkweather, C.K., Hassabis, D., Munos, R.,
738 and Botvinick, M. (2020). A distributional code for value in dopamine-based
739 reinforcement learning. Nature *577*, 671–675.

740 Eckstein, N., Bates, A.S., Du, M., Hartenstein, V., Jefferis, G.S.X., and Funke, J. (2020).
741 Neurotransmitter Classification from Electron Microscopy Images at Synaptic Sites in
742 Drosophila. bioRxiv.

743 Eschbach, C., Fushiki, A., Winding, M., Schneider-Mizell, C.M., Shao, M., Arruda, R.,
744 Eichler, K., Valdes-Aleman, J., Ohyama, T., Thum, A.S., et al. (2020). Recurrent
745 architecture for adaptive regulation of learning in the insect brain. Nat. Neurosci. *23*,
746 544–555.

747 Felsenberg, J., Barnstedt, O., Cognigni, P., Lin, S., and Waddell, S. (2017). Re-
748 evaluation of learned information in Drosophila. Nature *544*, 240–244.

749 Felsenberg, J., Jacob, P.F., Walker, T., Barnstedt, O., Edmondson-Stait, A.J., Pleijzier,
750 M.W., Otto, N., Schlegel, P., Sharifi, N., Perisse, E., et al. (2018). Integration of Parallel
751 Opposing Memories Underlies Memory Extinction. Cell *175*, 709–722.e15.

752 Gewirtz, J.C., and Davis, M. (1997). Second-order fear conditioning prevented by
753 blocking NMDA receptors in amygdala. Nature *388*, 471–474.

754 Gewirtz, J.C., and Davis, M. (2000). Using pavlovian higher-order conditioning
755 paradigms to investigate the neural substrates of emotional learning and memory. Learn.
756 Mem. 7, 257–266.

757 Gkanias, E., McCurdy, L.Y., Nitabach, M.N., and Webb, B. The incentive circuit: memory
758 dynamics in the mushroom body of Drosophila melanogaster.

759 Handler, A., Graham, T.G.W., Cohn, R., Morantte, I., Siliciano, A.F., Zeng, J., Li, Y., and
760 Ruta, V. (2019). Distinct Dopamine Receptor Pathways Underlie the Temporal
761 Sensitivity of Associative Learning. Cell *178*, 60–75.e19.

762 Hawkins, R.D., Greene, W., and Kandel, E.R. (1998). Classical conditioning, differential
763 conditioning, and second-order conditioning of the Aplysia gill-withdrawal reflex in a
764 simplified mantle organ preparation. Behavioral Neuroscience *112*, 636–645.

765 Helmstetter, F.J., and Fanselow, M.S. (1989). Differential second-order aversive
766 conditioning using contextual stimuli. Animal Learning & Behavior *17*, 205–212.

767 Hige, T., Aso, Y., Modi, M.N., Rubin, G.M., and Turner, G.C. (2015). Heterosynaptic
768 Plasticity Underlies Aversive Olfactory Learning in Drosophila. Neuron *88*, 985–998.

769 Holland, P.C. (1977). Conditioned stimulus as a determinant of the form of the Pavlovian
770 conditioned response. J. Exp. Psychol. Anim. Behav. Process. *3*, 77–104.

771 Huetteroth, W., Perisse, E., Lin, S., Klappenbach, M., Burke, C., and Waddell, S. (2015).
772 Sweet taste and nutrient value subdivide rewarding dopaminergic neurons in Drosophila.
773 Curr. Biol. *25*, 751–758.

774 Ichinose, T., Aso, Y., Yamagata, N., Abe, A., Rubin, G.M., and Tanimoto, H. (2015).
775 Reward signal in a recurrent circuit drives appetitive long-term memory formation. Elife
776 *4*, e10719.

777 Jacob, P.F., and Waddell, S. (2020). Spaced Training Forms Complementary Long-
778 Term Memories of Opposite Valence in Drosophila. Neuron *106*, 977–991.e4.

779 Jenett, A., Rubin, G.M., Ngo, T.-T.B., Shepherd, D., Murphy, C., Dionne, H., Pfeiffer,
780 B.D., Cavallaro, A., Hall, D., Jeter, J., et al. (2012). A GAL4-driver line resource for
781 Drosophila neurobiology. Cell Rep. *2*, 991–1001.

782 Jiang, L., and Litwin-Kumar, A. (2021) Models of heterogeneous dopamine signaling in
783 an insect learning and memory center. PLoS Comput Biol.. 10;17(8):e1009205.

784 Kim, H.F., Ghazizadeh, A., and Hikosaka, O. (2014). Separate groups of dopamine
785 neurons innervate caudate head and tail encoding flexible and stable value memories.
786 Front. Neuroanat. *8*, 120.

787 Kim, H.F., Ghazizadeh, A., and Hikosaka, O. (2015). Dopamine Neurons Encoding
788 Long-Term Memory of Object Value for Habitual Behavior. Cell *163*, 1165–1175.

789 Kim, S.D., Rivers, S., Bevins, R.A., and Ayres, J.J. (1996). Conditioned stimulus
790 determinants of conditioned response form in Pavlovian fear conditioning. J. Exp.
791 Psychol. Anim. Behav. Process. *22*, 87–104.

792 Kirkhart, C., and Scott, K. (2015). Gustatory learning and processing in the Drosophila
793 mushroom bodies. J. Neurosci. *35*, 5950–5958.

794 Klapoetke, N.C., Murata, Y., Kim, S.S., Pulver, S.R., Birdsey-Benson, A., Cho, Y.K.,
795 Morimoto, T.K., Chuong, A.S., Carpenter, E.J., Tian, Z., et al. (2014). Independent
796 optical excitation of distinct neural populations. Nat. Methods *11*, 338–346.

797 König, C., Khalili, A., Niewalda, T., Gao, S., and Gerber, B. (2019). An optogenetic
798 analogue of second-order reinforcement in Drosophila. Biol. Lett. *15*, 20190084.

799 Krashes, M.J., and Waddell, S. (2008). Rapid consolidation to a radish and protein
800 synthesis-dependent long-term memory after single-session appetitive olfactory
801 conditioning in Drosophila. J. Neurosci. *28*, 3103–3113.

802 Lewis, L.P.C., Siju, K.P., Aso, Y., Friedrich, A.B., Bulteel, A.J.B., Rubin, G.M., and
803 Grunwald Kadow, I.C. (2015). A Higher Brain Circuit for Immediate Integration of
804 Conflicting Sensory Information in Drosophila. Curr. Biol. *25*, 2203–2214.

805 Li, F., Lindsey, J.W., Marin, E.C., Otto, N., Dreher, M., Dempsey, G., Stark, I., Bates,
806 A.S., Pleijzier, M.W., Schlegel, P., et al. (2020). The connectome of the adult Drosophila
807 mushroom body provides insights into function. Elife *9*.

808 Lin, S., Owald, D., Chandra, V., Talbot, C., Huetteroth, W., and Waddell, S. (2014).
809 Neural correlates of water reward in thirsty Drosophila. Nat. Neurosci. *17*, 1536–1542.

810 Liu, W.W., and Wilson, R.I. (2013). Glutamate is an inhibitory neurotransmitter in the
811 Drosophila olfactory system. Proc. Natl. Acad. Sci. U. S. A. *110*, 10294–10299.

812 Liu, C., Plaçais, P.-Y., Yamagata, N., Pfeiffer, B.D., Aso, Y., Friedrich, A.B., Siwanowicz,
813 I., Rubin, G.M., Preat, T., and Tanimoto, H. (2012). A subset of dopamine neurons
814 signals reward for odour memory in Drosophila. Nature *488*, 512–516.

815 Maes, E.J.P., Sharpe, M.J., Usypchuk, A.A., Lozzi, M., Chang, C.Y., Gardner, M.P.H.,
816 Schoenbaum, G., and Iordanova, M.D. (2020). Causal evidence supporting the proposal
817 that dopamine transients function as temporal difference prediction errors. Nat.
818 Neurosci. 23, 176–178.

819 McCurdy, L.Y., Sareen, P., Davoudian, P.A., and Nitabach, M.N. (2021). Dopaminergic
820 mechanism underlying reward-encoding of punishment omission during reversal learning

821 in Drosophila. Nat. Commun. *12*, 1115.

822 Mizunami, M., Unoki, S., Mori, Y., Hirashima, D., Hatano, A., and Matsumoto, Y. (2009).
823 Roles of octopaminergic and dopaminergic neurons in appetitive and aversive memory
824 recall in an insect. BMC Biol. *7*, 1–16.

825 Nern, A., Pfeiffer, B.D., and Rubin, G.M. (2015). Optimized tools for multicolor stochastic
826 labeling reveal diverse stereotyped cell arrangements in the fly visual system. Proc. Natl.
827 Acad. Sci. U. S. A. *112*, E2967–E2976.

828 Owald, D., and Waddell, S. (2015). Olfactory learning skews mushroom body output
829 pathways to steer behavioral choice in Drosophila. Curr. Opin. Neurobiol. *35*, 178–184.

830 Pai, T.-P., Chen, C.-C., Lin, H.-H., Chin, A.-L., Lai, J.S.-Y., Lee, P.-T., Tully, T., and
831 Chiang, A.-S. (2013). Drosophila ORB protein in two mushroom body output neurons is
832 necessary for long-term memory formation. Proc. Natl. Acad. Sci. U. S. A. *110*, 7898–
833 7903.

834 Pavlov, I.P. (1927). Lectures on conditioned reflexes: Twenty-five years of objective
835 study of the higher nervous activity (behaviour) of animals (New York).

836 Pettersson, J. (1970). An Aphid Sex Attractant. Insect Systematics & Evolution *1*, 63–73.

837 Pfeiffer, B.D., Ngo, T.-T.B., Hibbard, K.L., Murphy, C., Jenett, A., Truman, J.W., and
838 Rubin, G.M. (2010). Refinement of tools for targeted gene expression in Drosophila.
839 Genetics *186*, 735–755.

840 Plaçais, P.-Y., Trannoy, S., Isabel, G., Aso, Y., Siwanowicz, I., Belliart-Guérin, G.,
841 Vernier, P., Birman, S., Tanimoto, H., and Preat, T. (2012). Slow oscillations in two pairs
842 of dopaminergic neurons gate long-term memory formation in Drosophila. Nat. Neurosci.
843 *15*, 592–599.

844 Plaçais, P.-Y., Trannoy, S., Friedrich, A.B., Tanimoto, H., and Preat, T. (2013). Two
845 pairs of mushroom body efferent neurons are required for appetitive long-term memory
846 retrieval in Drosophila. Cell Rep. *5*, 769–780.

847 Rescorla, R.A. (1980). Pavlovian Second-order Conditioning: Studies in Associative
848 Learning (Psychology Press).

849 Rescorla, R.A., and Furrow, D.R. (1977). Stimulus similarity as a determinant of
850 Pavlovian conditioning. J. Exp. Psychol. Anim. Behav. Process. *3*, 203–215.

851 Riemensperger, T., Völler, T., Stock, P., Buchner, E., and Fiala, A. (2005). Punishment
852 prediction by dopaminergic neurons in Drosophila. Curr. Biol. *15*, 1953–1960.

853 Roeper, J. (2013). Dissecting the diversity of midbrain dopamine neurons. Trends
854 Neurosci. *36*, 336–342.

855 Scheffer, L.K., Xu, C.S., Januszewski, M., Lu, Z., Takemura, S.-Y., Hayworth, K.J.,
856 Huang, G.B., Shinomiya, K., Maitlin-Shepard, J., Berg, S., et al. (2020). A connectome
857 and analysis of the adult central brain. Elife *9*.

858 Schultz, W. (1998). Predictive Reward Signal of Dopamine Neurons. Journal of

Neurophysiology *80*, 1–27.

Séjourné, J., Plaçais, P.-Y., Aso, Y., Siwanowicz, I., Trannoy, S., Thoma, V., Tedjakumala, S.R., Rubin, G.M., Tchénio, P., Ito, K., et al. (2011). Mushroom body efferent neurons responsible for aversive olfactory memory retrieval in Drosophila. Nat. Neurosci. *14*, 903–910.

Shannon, P., Markiel, A., Ozier, O., Baliga, N.S., Wang, J.T., Ramage, D., Amin, N., Schwikowski, B., and Ideker, T. (2003). Cytoscape: a software environment for integrated models of biomolecular interaction networks. Genome Res. *13*, 2498–2504.

Siju, K.P., Štih, V., Aimon, S., Gjorgjieva, J., Portugues, R., and Grunwald Kadow, I.C. (2020). Valence and State-Dependent Population Coding in Dopaminergic Neurons in the Fly Mushroom Body. Curr. Biol. *30*, 2104–2115.e4.

Stanhope, K.J. (1992). The representation of the reinforcer and the force of the pigeon's keypeck in first- and second-order conditioning. Q. J. Exp. Psychol. B *44*, 137–158.

Starkweather, C.K., and Uchida, N. (2021). Dopamine signals as temporal difference errors: recent advances. Curr. Opin. Neurobiol. *67*, 95–105.

Sun, F., Zhou, J., Dai, B., Qian, T., Zeng, J., Li, X., Zhuo, Y., Zhang, Y., Wang, Y., Qian, C., et al. (2020). Next-generation GRAB sensors for monitoring dopaminergic activity in vivo. Nat. Methods *17*, 1156–1166.

Tabone, C.J., and de Belle, J.S. (2011). Second-order conditioning in Drosophila. Learn. Mem. *18*, 250–253.

Takeda, K. (1961). Classical conditioned response in the honey bee. J. Insect Physiol. *6*, 168–179.

Tanaka, N.K., Tanimoto, H., and Ito, K. (2008). Neuronal assemblies of the Drosophila mushroom body. J. Comp. Neurol. *508*, 711–755.

Tanimoto, H., Heisenberg, M., and Gerber, B. (2004). Experimental psychology: event timing turns punishment to reward. Nature *430*, 983.

Tempel, B.L., Bonini, N., Dawson, D.R., and Quinn, W.G. (1983). Reward learning in normal and mutant Drosophila. Proc. Natl. Acad. Sci. U. S. A. *80*, 1482–1486.

Tully, T., and Quinn, W.G. (1985). Classical conditioning and retention in normal and mutant Drosophila melanogaster. J. Comp. Physiol. A *157*, 263–277.

Ueoka, Y., Hiroi, M., Abe, T., and Tabata, T. (2017). Suppression of a single pair of mushroom body output neurons in Drosophila triggers aversive associations. FEBS Open Bio *7*, 562–576.

Vrontou, E., Groschner, L.N., Szydlowski, S., Brain, R., Krebbers, A., and Miesenböck, G. (2021). Response competition between neurons and antineurons in the mushroom body. Curr. Biol. *31*, 4911–4922.e4.

Wan, Y., Otsuna, H., Chien, C.-B., and Hansen, C. (2012). FluoRender: An Application of 2D Image Space Methods for 3D and 4D Confocal Microscopy Data Visualization in

Neurobiology Research. IEEE Pac. Vis. Symp. 201–208.

Watabe-Uchida, M., and Uchida, N. (2018). Multiple Dopamine Systems: Weal and Woe of Dopamine. Cold Spring Harb. Symp. Quant. Biol. *83*, 83–95.

Worden, B.D., and Papaj, D.R. (2005a). Flower choice copying in bumblebees. Biol. Lett. *1*, 504–507.

Worden, B.D., and Papaj, D.R. (2005b). Flower choice copying in bumblebees. Biol. Lett. *1*, 504–507.

Yamagata, N., Ichinose, T., Aso, Y., Plaçais, P.-Y., Friedrich, A.B., Sima, R.J., Preat, T., Rubin, G.M., and Tanimoto, H. (2015). Distinct dopamine neurons mediate reward signals for short- and long-term memories. Proc. Natl. Acad. Sci. U. S. A. *112*, 578–583.

Zheng, Z., Lauritzen, J.S., Perlman, E., Robinson, C.G., Nichols, M., Milkie, D., Torrens, O., Price, J., Fisher, C.B., Sharifi, N., et al. (2018). A Complete Electron Microscopy Volume of the Brain of Adult Drosophila melanogaster. Cell *174*, 730–743.e22.

Zolin, A., Cohn, R., Pang, R., Siliciano, A.F., Fairhall, A.L., and Ruta, V. (2021). Context-dependent representations of movement in Drosophila dopaminergic reinforcement pathways. Nat. Neurosci. *24*, 1555–1566.

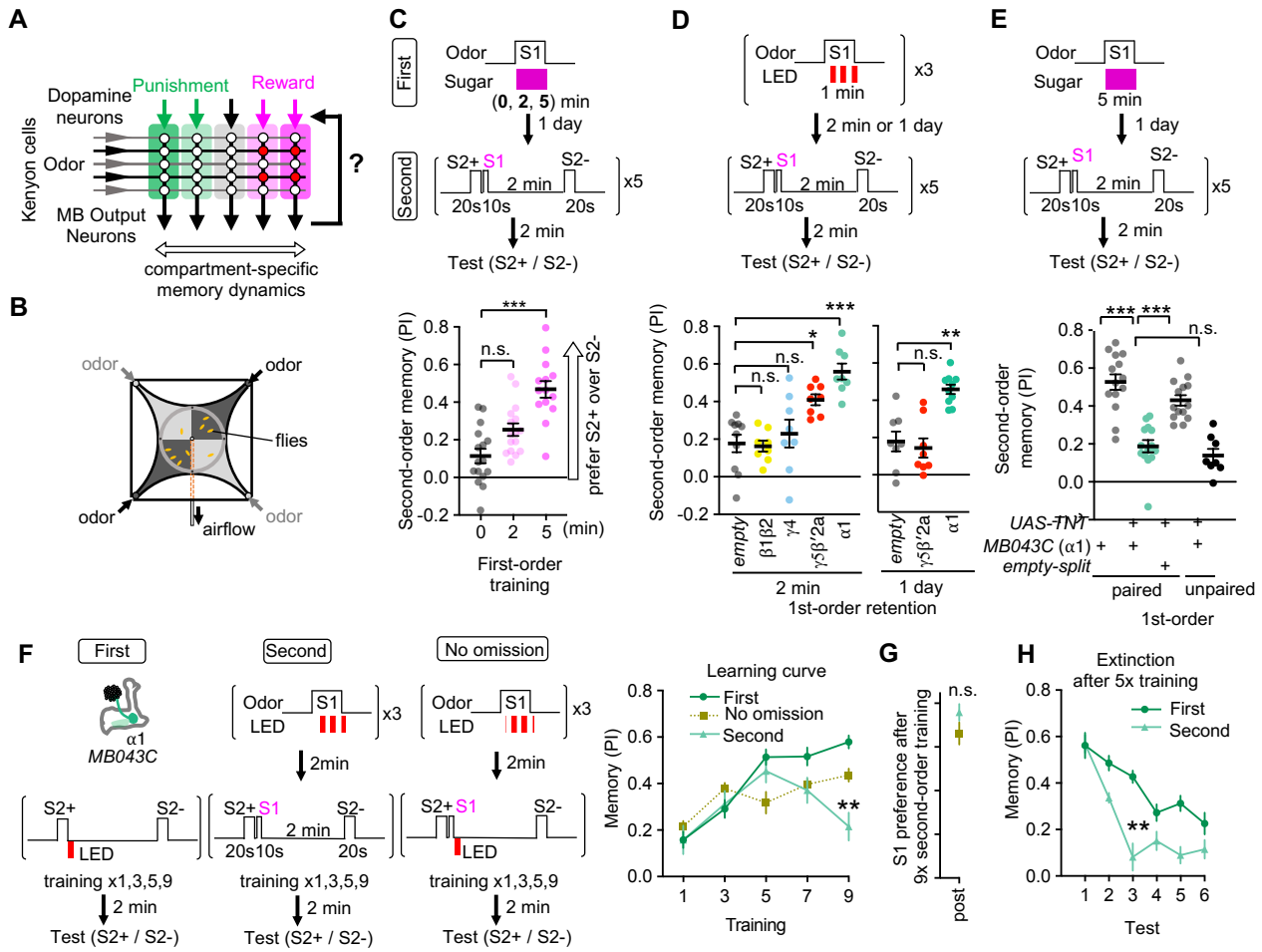

Figure 1 Appetitive olfactory second-order conditioning in Drosophila

(A) A simplified diagram of the mushroom body circuit. Identity of odors are encoded by patterns of activity in ~2,000 Kenyon cells. Contingent activity of Kenyon cells and dopamine release leads to plasticity of excitatory synapses from Kenyon cells to MB output neurons with compartment-specific dynamics.

(B) A diagram of the four-armed olfactory arena. Flies were confined in the 9 cm diameter circular area above the LED board. For odor-sugar conditioning, flies were first trained in a tube by pairing an odor with dried sugar paper, and then introduced to the olfactory arena. Performance index was calculated by counting the number of flies in each quadrant (see Methods).

(C) Second-order memory performance by wild type flies. n.s., not significant; ***, p<0.001; Dunn's multiple comparison tests following Kruskal-Wallis test; N = 14–16. Means and SEMs are displayed with individual data points.

(D) The second-order conditioning 2-min or 1 day after the first-order conditioning with optogenetic activation of various DAN types (see Figure 1-figure supplement 2C). Second-order memory was tested immediately after pairing S2+ odor with S1 odor (MCH) five times. n.s., not significant; *, p<0.05; ***, p<0.001 ; Dunn's multiple comparison tests following Kruskal-Wallis test; N=8-10.

(E) Flies expressing TNT with MB043C split-GAL4 showed impaired second-order memory compared to genetic controls. For unpaired control, 5-min sugar was ended 2-min prior to the onset of S1 odor. ***, p<0.001; Dunn's multiple comparison tests following Kruskal-Wallis test; N=14 for paired and N=8 for unpaired.

(F) Learning curves by first-order, second-order, or second-order without omission of optogenetic reward. Flies expressing CsChrimson with MB043C split-GAL4 were trained by pairing S2+ odor directly with optogenetic activation of DANs (First) or S1 odor that was previously paired with DAN activation (Second). In the no omission protocol, DANs were activated immediately after S1 by repeating 1s red LED illumination with 1s intervals for three times. Preference between S2+ and S2- odors was tested after 1st, 3rd, 5th, 7th and 9th training sessions. After 9th training, memory by second-order protocol was lower than other protocols and its peak at 5th training. **, p<0.01; Dunn's multiple comparison tests following Kruskal-Wallis test; N=8-10.

(G) The preference for the S1 odor (MCH) after the 9th session of second-order conditioning as in F. n.s., not significant; Mann-Whitney test; N=8.

(H) Comparison of memory decay after repetitive tests. Flies were trained five times with first or second-order conditioning protocol as in F but without tests. Immediately after the 5th training, preference between two S2 odors was measured repeatedly without training. At third test, second-order memory was significantly lower than first-order memory. **, p<0.01; Dunn's multiple comparison tests following Kruskal-Wallis test; N=8.

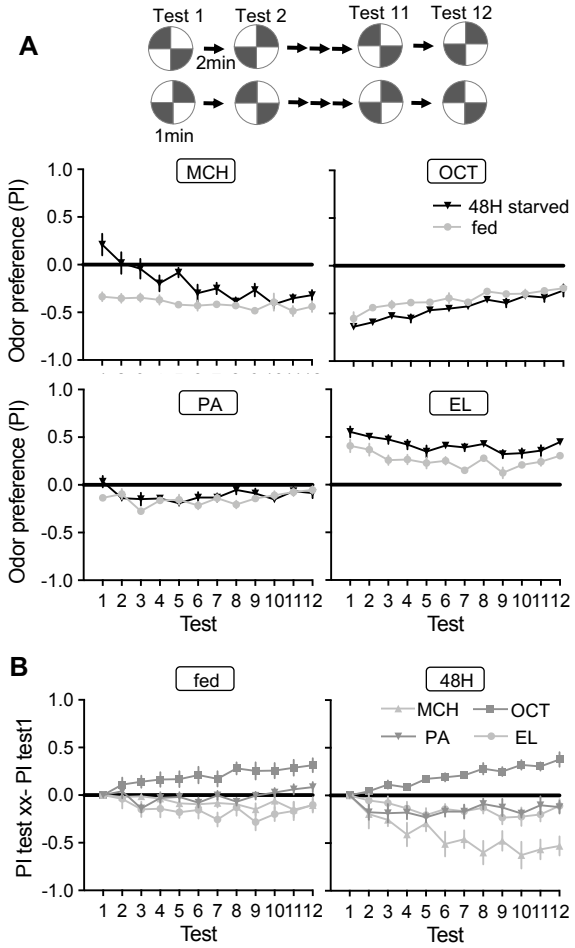

Figure 1-figure supplement 1 Dynamics of odor preference
(A)Twelve repetition of odor preference of fed and 40-48 hour starved flies.
PIs represent results of reciprocal experiments. The half groups of flies went through the identical tests but with alternating positions of odors and air quadrants to cancel out potential positional preference for each rigs. The mean odor preferences during 12 tests were significantly different between fed and starved flies for MCH and EL. $p<0.01$; unpaired t-test; N=8. Means and SEM are shown.
(B) Delta between the first test and subsequent tests in fed (left) and 40-48 hour starved flies (right). Areas under curve for OCT was significantly higher than that for other odors in both fed and starve flies, whereases the area under the curve for MCH was lower than other odors only in starved flies. $p<0.01$; unpaired t-test; N=8.

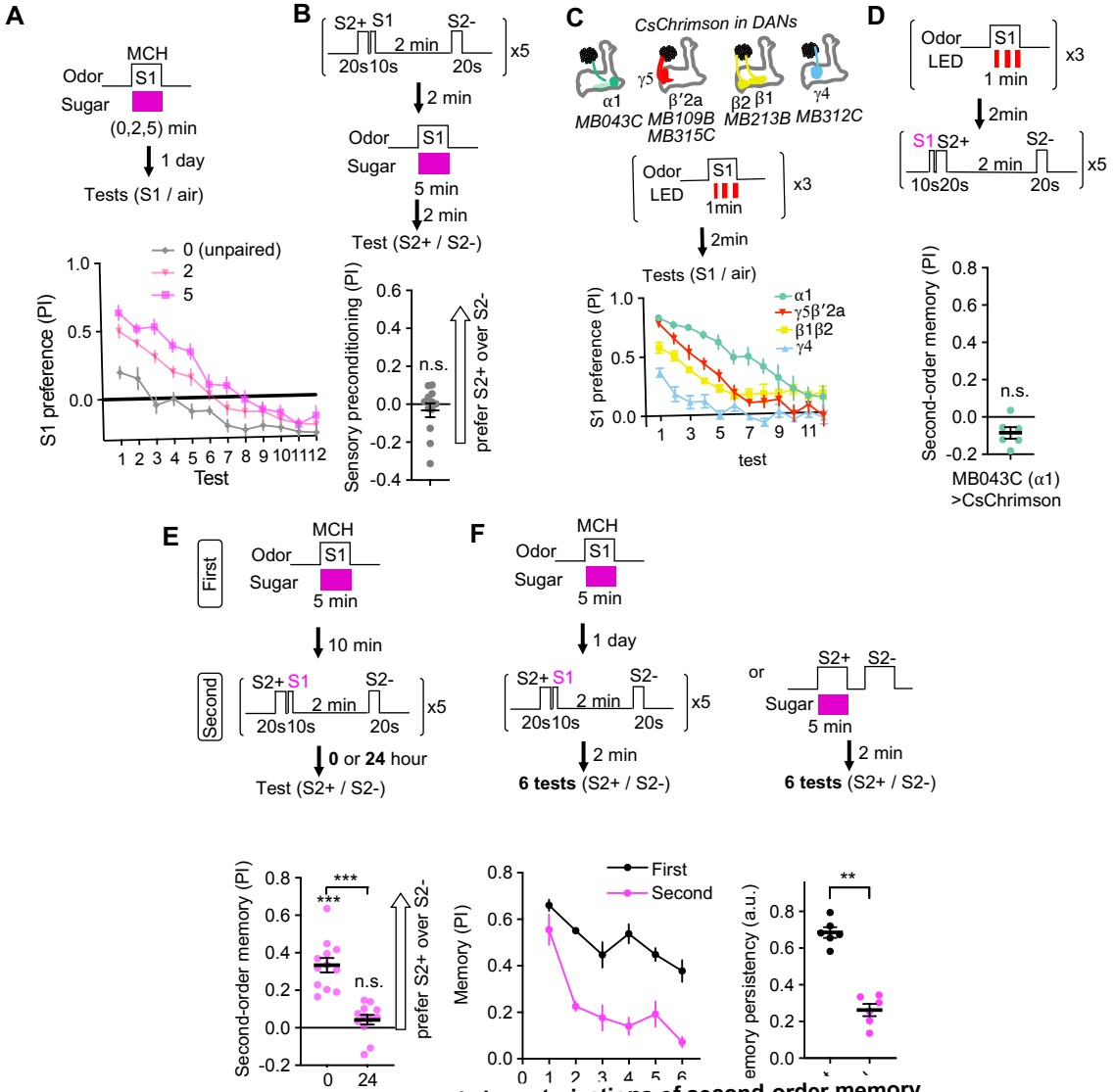

Figure 1-figure supplement 2 Controls and characterizations of second-order memory

(A) Dynamics of MCH preference after various 2 or 5 min of first-order conditioning with sugar. Flies were trained after 40-48 hours of starvation and memories were tested 20-24 hours later without feeding in between by examining preference to MCH over air for 12 times. Unpaired group received 5 min of sugar 2 min prior to 5 min exposure to MCH. Mean performance index of the first 5 tests after 5 min training was higher than that of 2 min. $p<0.01$; unpaired t-test; N=10-12.

(B) The odor preference following the sensory preconditioning protocol, in which the order of the first and second-order conditioning was swapped. n.s., not significantly different from the chance level; Wilcocxon signed-rank test; N=12.

(C) Dynamics of S1 odor (MCH) preference after pairing 1 min of S1 odor with activation of different PAM cluster DANs with CsChrimson-mVenus for three times. At 3rd-7th tests, MCH preference of MB043C>CsChrimson flies was higher than all other genotypes. $p<0.05$; Dunn's multiple comparison tests following Kruskal-Wallis test; N=6.

(D) The second-order memory immediately after backward second-order conditioning. Flies expressing CsChrimon-mVenus by MB043C split-GAL4 were trained with identical protocol as in Figure 1D, except that the onset of S1 odor was shifted to the 10 second before the onset of the first S2 odor. n.s., not significant from zero; Wilcocxon signed-rank test; N=6.

(E) Retention of second-order memory. After 24-hour, the second-order memory decayed to the chance level. ***, $p<0.001$; Wilcocxon signed-rank test or Mann-Whiteney test; N = 12.

(F) Odor preference between two S2 odors after the second-order or first-order conditioning was measured for six times by alternative position of two odorants with 2 min intervals. Memory persistency, a mean of PIs for 3rd-6th tests divided by PI of 1st test, was significantly smaller for second-order memory. **; $p<0.01$; Mann-Whitney test; N=6. Means and SEMs are displayed with individual data points.

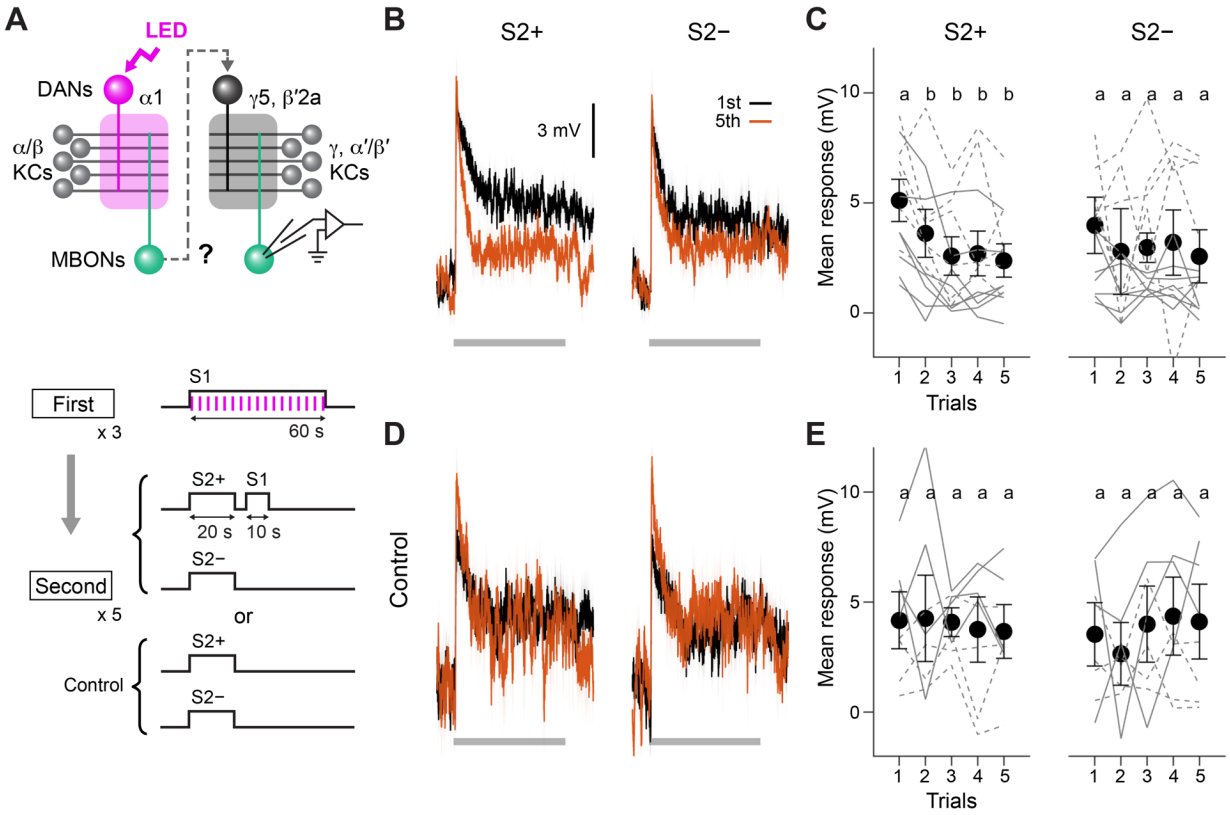

Figure 2. Second-order conditioning induces cross-compartmental plasticity.

(A) Experimental design and protocol. ChrimsonR-mVenus was selectively expressed in PAM-α1 using MB043-split-LexA (*58E02-ZpLexADBD in JK22C; 32D11-p65ADZp in JK73A)*, and in vivo whole-cell recordings were made from MBON-γ5β′2a, which was labeled by mScarlet using a split-GAL4 driver *SS01308*. For the first-order conditioning, 1-min presentation of S1 (MCH) was paired with LED stimulation (1 ms, 2 Hz, 120 times), which caused odor-specific suppression of responses in MBON-a1 (Figure 2-figure supplement 1). After repeating first-order conditioning three times with 2-min intervals, second-order conditioning was performed by presenting S2+ (either PA or EL) for 20 s, and then S1 for 10 s with 5-s delay. S2− was presented alone 2 min later. Second-order conditioning was repeated five times, and the responses to S2 were recorded. In control experiments, first-order conditioning was performed in the same manner, but the presentation of S1 was omitted during second-order conditioning. Reciprocal experiments were performed by swapping S2+ and S2− in separate flies.
(B) Mean responses (± SEM) to S2+ and S2− in the first (black) and fifth trials (red) during second-order conditioning (n = 14, including reciprocal experiments).
(C) Mean response magnitudes (± SEM) evoked by S2+ and S2−. Each solid (PA used as S2+; n = 7) and dashed line (EL as S2+; n = 7) indicates data from a single fly. Responses to S2+ underwent depression after the first trial, while those to S2− did not change. Different letters indicate significant differences detected by Tukey's post hoc multiple comparisons test ($p < 0.05$) following repeated-measures two-way ANOVA ($p = 0.003$).
(D, E) Same as (B) and (C) except that the data are from control experiments (n = 4 each with PA or EL used as S2+, respectively). Neither responses to S2+ nor S2− changed ($p = 0.28$; repeated-measures two-way ANOVA).

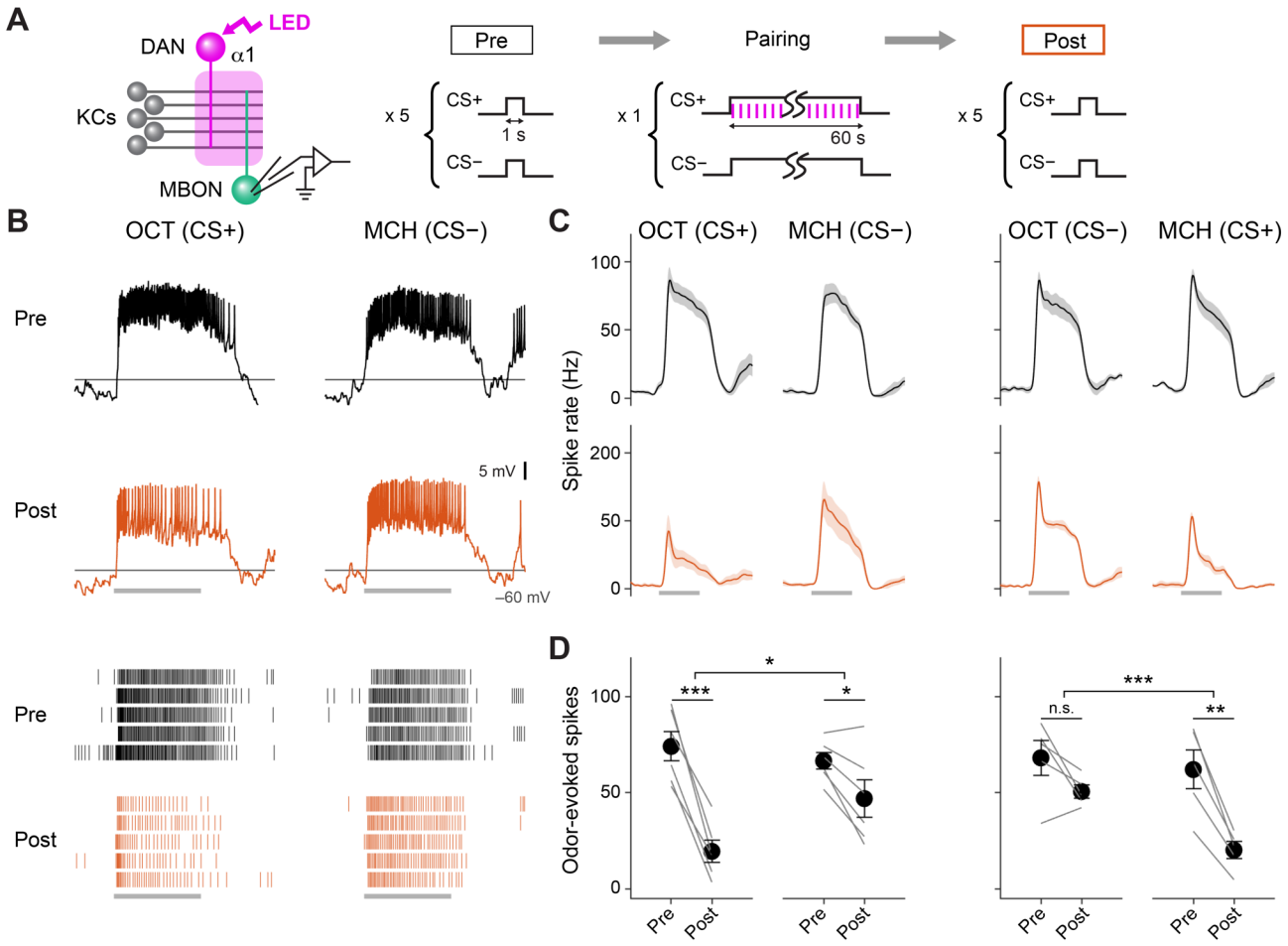

Figure 2-figure supplement 1 Optogenetic Conditioning in α1 Compartment Induces Depression in MBON-α1
(A) Experimental design and protocol. ChrimsonR-mVenus was selectively expressed in PAM-α1 using MB043-split-LexA, and in vivo whole-cell recordings were made from MBON-α1, which was labeled by mScarlet using a split-GAL4 driver MB319C. 1-min presentation of CS+ (OCT or MCH) was paired with LED stimulation (1 ms, 2 Hz, 120 times), followed by 1-min presentation of CS− alone. Reciprocal experiments were performed by swapping CS+ and CS− in a separate set of flies.
(B) Membrane voltage (upper panels) and spike data (lower panels) from a single representative fly, in which OCT was used as CS+. Gray bars indicate 1-s odor presentation.
(C) Time courses of instantaneous spike rate (mean ± SEM; n = 6 and 5 for each set of experiment).
(D) Summary data of mean odor-evoked spike counts (± SEM). Gray lines indicate data from individual neurons. After each pairing, responses to CS+ were suppressed, while those to CS− were either showed less suppression than CS+ or no change (repeated-measures two-way ANOVA followed by Tukey's post hoc multiple comparisons test; *p < 0.05, **p < 0.005, ***p < 0.001).

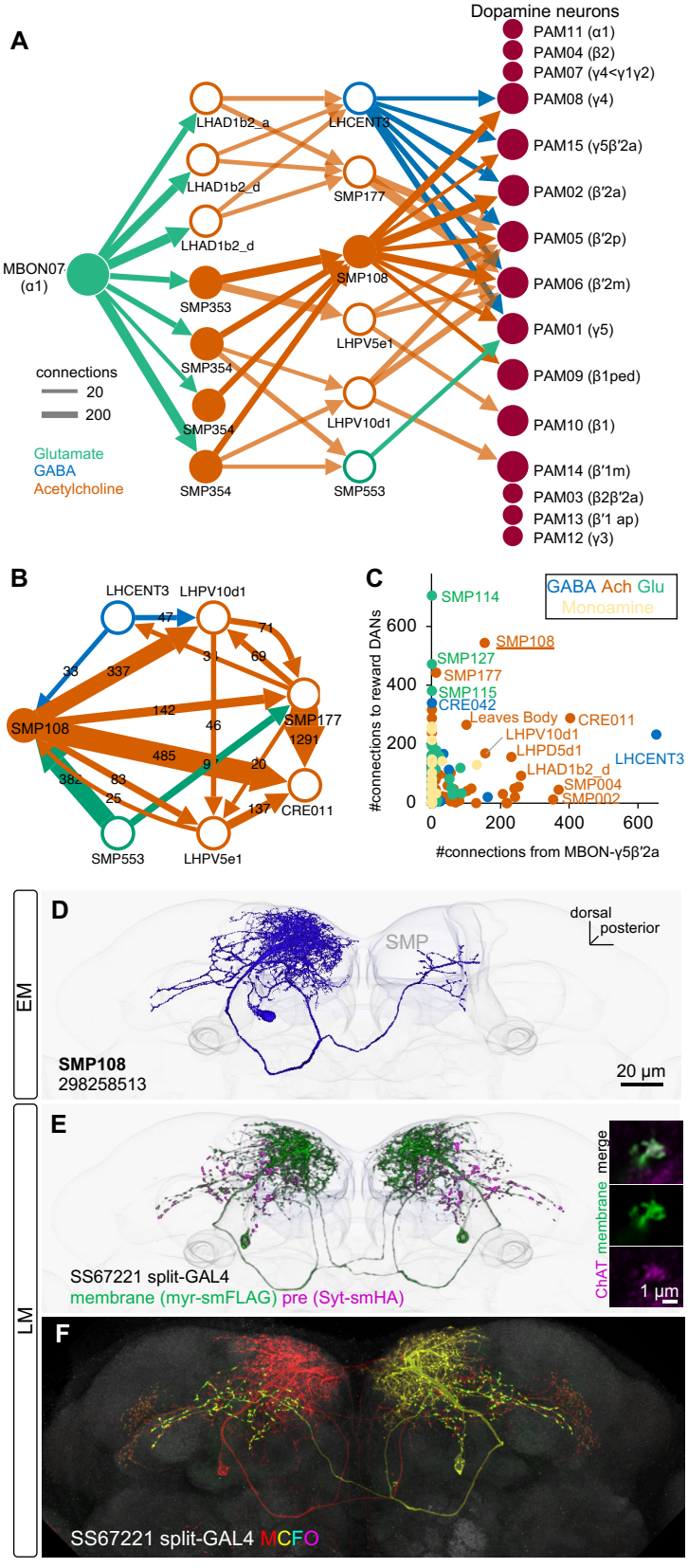

Figure 3 SMP108 is a key interneuron between MBON-α1 and DANs

(A)The connections from MBON-α1 to PAM cluster DANs with two interneurons identified in the hemibrain EM data (Scheffer et al., 2020). The width of arrows indicate number of connections. The colors of circles and arrows indicate type of putative neurotransmitter. Single SMP353 and three SMP354s have similar morphology and projection patterns and converge on to SMP108. Cholinergic interneurons SMP353/SMP354 and SMP108 are shown as filled orange circles and arrows. Other cholinergic connections are shown in transparent orange. See Supplementary File 1 for a full connectivity matrix and neurotransmitter predictions.

(B) Connections between the six neurons in the second layer in A and CRE011. SMP108 outputs to all three other putative cholinergic interneurons. LHPV10d1 is the top target of SMP108. SMP553 send its first and second strongest outputs to SMP108 and SMP177.

(C) Total number of connections to reward DANs (PAM01, 02, 04, 06, 07, 08, 10, 11,15) which can induce appetitive memory with optogenetic activation, plotted against number of inputs from MBON-γ5β′2a. Each circle represents one of 396 interneuron cell types that have at least 100 total connections with MBONs and DANs. Similar to SMP108, CRE011 is an outlier cell type in terms of high number of direct inputs from MBON-γ5β′2a and outputs to reward DANs.

(D) A projection of a reconstructed SMP108 neuron in the hemibrain EM images aligned to a standard brain with outline of brain and the MB lobes.

(E) Confocal microscope images of SS67221 split-GAL4 driver with membrane-targeted reporter myr-smFLAG and presynaptic reporter Syt-smHA. Inset shows anti-ChAT immunoreactivity of SMP108's axon terminals.

(F) Morphology of individual SMP108 visualized by multi-color flip out of SS67221 split-GAL4.

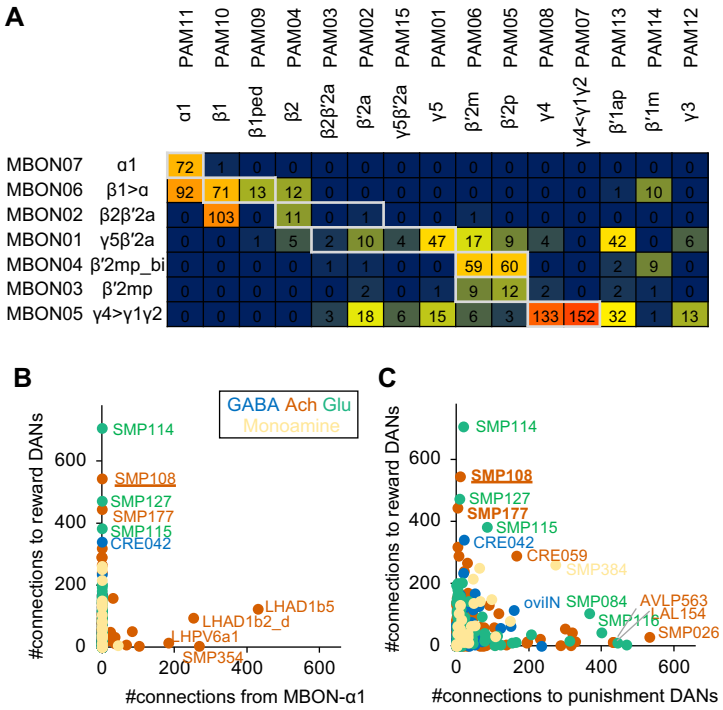

Figure 3-figure supplement 1 Connections of MBON-α1 and SMP108
(A) Numbers of direct MBON-to-DANs synaptic connections. White boxes indicate within-a-compartment connection such as connection from MBON-α1 to PAM-α1.
(B) Total number of outputs to reward DANs (i.e. PAM01, 02, 04, 06, 07, 08, 10, 11,15) which can induce appetitive memory upon optogenetic activation, plotted against total number of connection from MBON-α1 for 396 cell types that have at least 100 total connections with MBONs and DANs. Colors indicate predicted neurotransmitters. One of outstanding cell type, LHAD1b5, cannot mediate cross-compartmental pathways because it is exclusively connected with PAM-α1 but not other reward DANs. Another outstanding cell type LHAD1b2_d is a part of two-hop pathways from MBON-α1 to PAM-α1 (Figure 3A)
(C) Total number of outputs to reward DANs plotted against total number of outputs to punishment DANs (i.e. PPL101, 103, 105, 106 and PAM12).

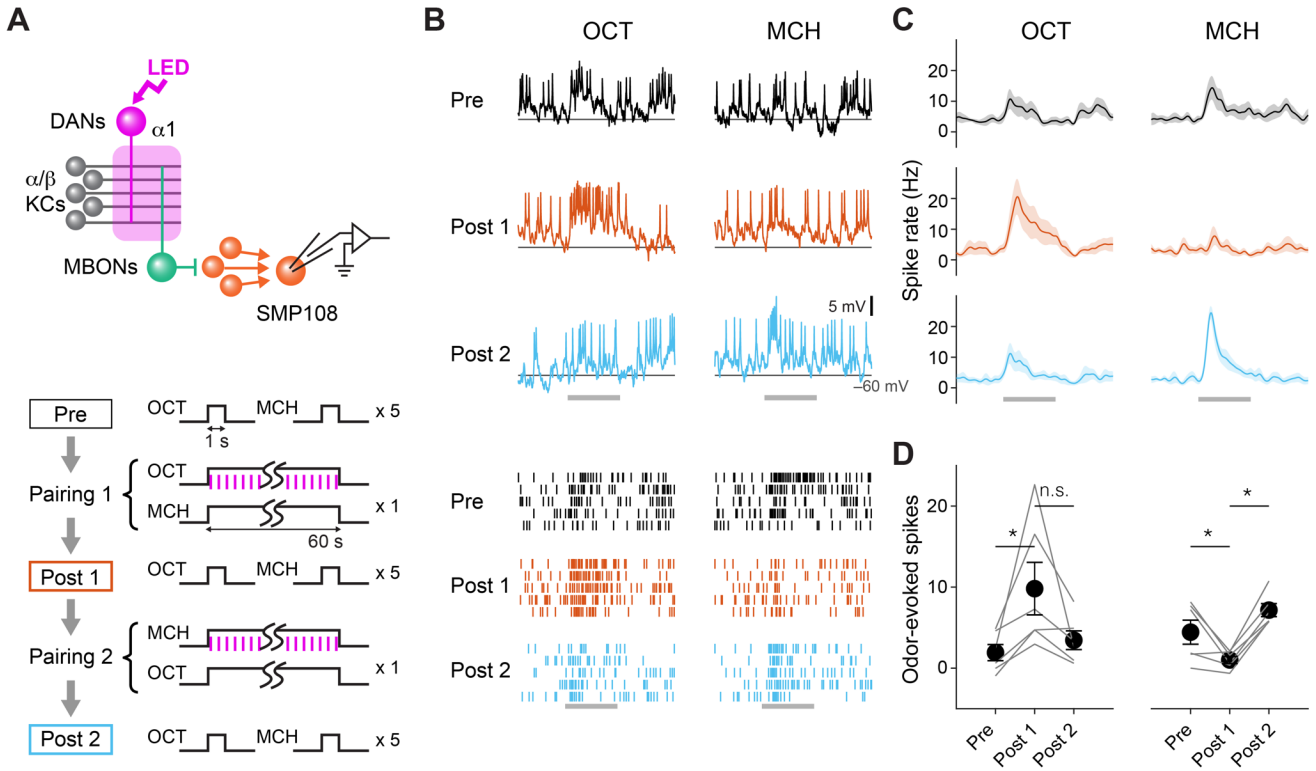

Figure 4. SMP108 acquires enhanced responses to reward-predicting odors
(A) Experimental design and protocol. ChrimsonR-mVenus was expressed in PAM-cluster DANs, which include PAM-α1, using R58E02-LexA. In vivo whole-cell recordings were made from SMP108, which was labeled by GFP using a split-GAL4 driver SS45234. In the first pairing (Pairing 1), 1-min presentation of OCT was paired with LED stimulation (1 ms, 2 Hz, 120 times), followed by 1-min presentation of MCH alone. Odors were flipped in the second round of pairing (Pairing 2). Responses to each odor (1-s presentation) were measured before (Pre) and after pairing 1 (Post 1), and after pairing 2 (Post 2).
(B) Membrane voltage (upper panels) and spike data (lower panels) from a single representative neuron. Gray bars indicate 1-s odor presentation.
(C) Time courses of instantaneous spike rate (mean ± SEM; n = 6).
(D) Summary data of mean odor-evoked spike counts (± SEM). Gray lines indicate data from individual neurons. After each pairing, responses to paired odors were potentiated, while those to unpaired odors tended to decrease. Repeated-measures two-way ANOVA ($p = 0.0001$) followed by Tukey's post hoc multiple comparisons test. *$p < 0.05$.

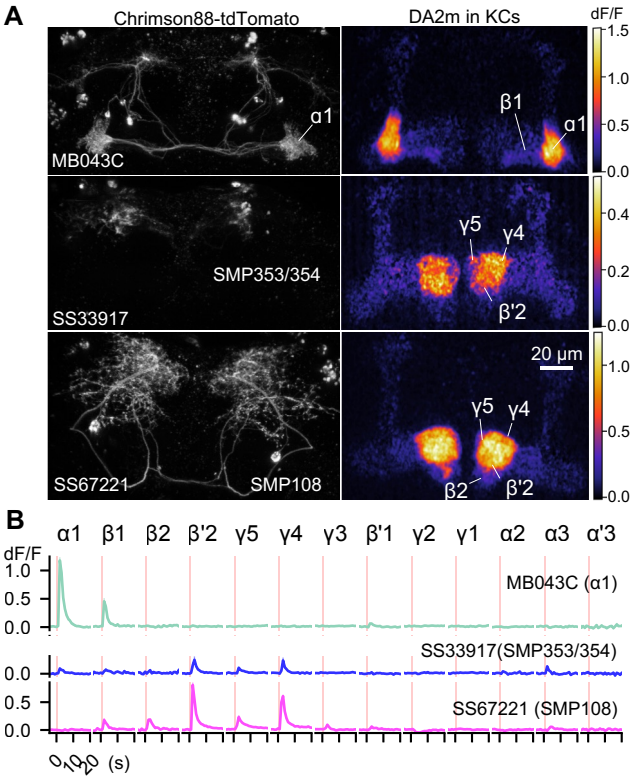

Figure 5 SMP108 promotes dopamine release in multiple compartments

(A) Representative images of Chrimson88-tdTtomato expression patterns (left) and maximum intensity projections of DA2m dF/F in the MB lobes (right). Release of dopamine upon activation of DANs or SMP108 pathways, measured with dopamine sensor DA2m expressed in Kenyon cells. *10XUAS-Syn21-Chrimson88-tdTtomato-3.1 in attP18* was driven with designated split-GAL4 driver lines. Fluorescence of DA2m in response to one second of 660nm LED light was measured in dissected brains with two-photon imaging of volume containing MB lobes (see Methods).

(B) Mean DA2m dF/F in ROIs defined for each MB compartment. SEMs are shown as shading, although they are often within width of lines representing means. N=8-12.

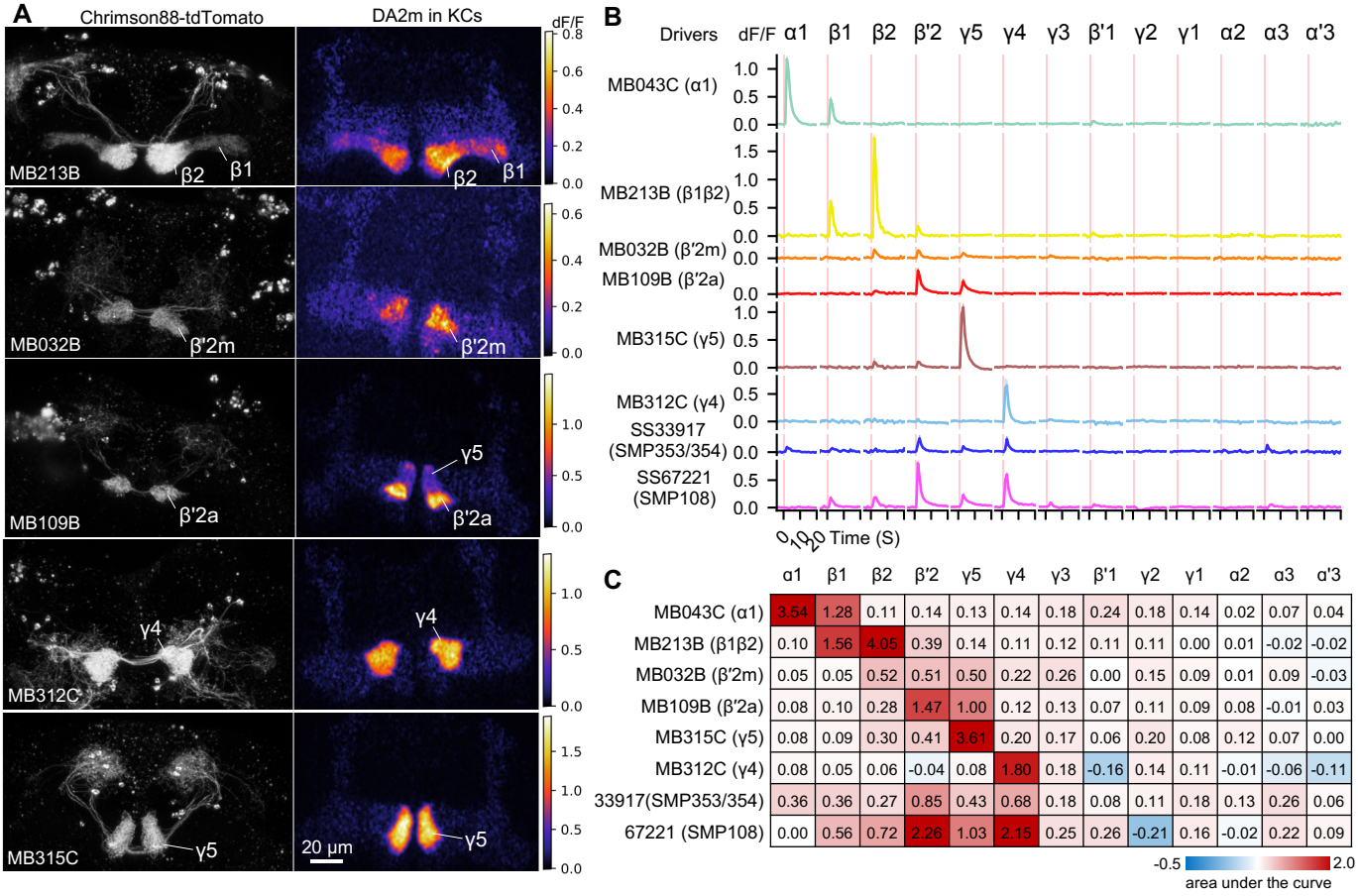

Figure 5-figure supplement 1 Patterns of dopamine release by different driver lines
Representative images of neurons expressing Chrimson88-tdTtomato by designated driver lines (left) and maximum intensity projection of DA2m dF/F in the MB lobes (right).
(A) Representative images of Chrimson88-tdTtomato expression patterns (left) and max intensity projections of DA2m dF/F in the MB lobes (right) as in Figure 5A.
(B) Mean DA2m dF/F in ROIs defined for each MB compartment. N=8-12.
(C) Area under the curve during the 10s period after activation.

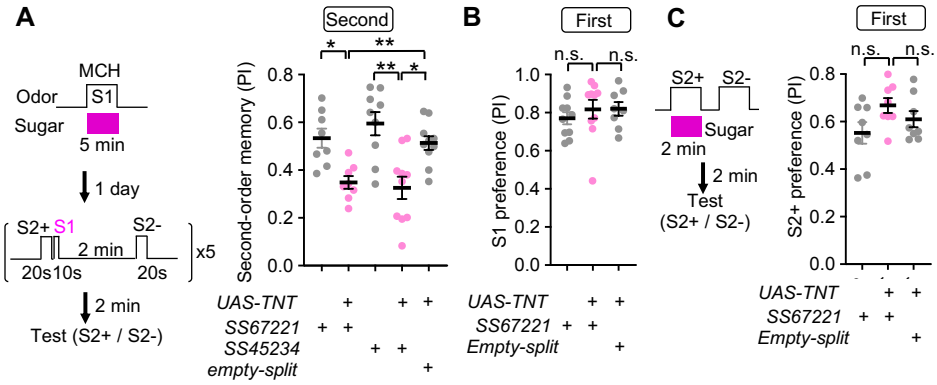

Figure 6 SMP108 is required for second-order memory

(A) Second-order memory immediately after 5 training sessions as in Figure 1C following 5min first order conditioning a day before. Blocking SMP108 by expressing TNT with SS67221 or SS45234 impaired the second-order memory compared to genetic controls. N=10-12.

(B) Preference to the S1 (MCH) odor one day after pairing with sugar for 5min. N=8-10.

(C) First-order memory immediately after pairing S2+ odor with sugar for 2-min. N=8. *, p<0.05; **, p<0.01; Dunn's multiple comparison tests following Kruskal-Wallis test;

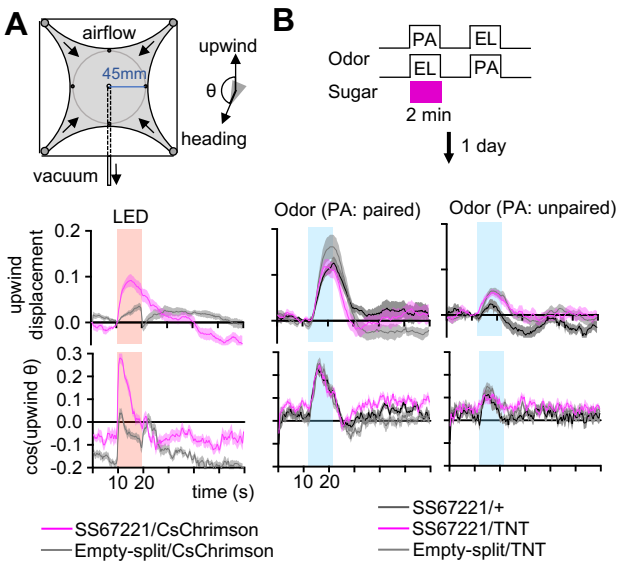

Figure 6-figure supplement 1 SMP108 can drive upwind steering but dispensable for the conditioned responses

(A) Diagram of the circular arena (top). Airflow was constantly set at 400mL/min throughout the experiments, and 10s of 627nm LED stimulations was applied for six times with 2min intervals. Six trial averages of upwind displacement from the onset of LED (middle) and cosine of angle to upwind direction (bottom) are shown for flies expressing CsChrimson SS67221 (SMP108) or empty-split-GAL4. SS67221>CsChrimson flies showed enhanced upwind displacement ($p<0.05$) and orientation toward upwind during LED ON period ($p<0.01$); See the method for the calculation of upwind displacement. N=12.

(B) Groups of flies were trained by pairing either PA or EL with sugar for 2-min, and their response to airflow in the presence of odors were examined 20-24 hours later. Flies showed enhanced upwind displacement and orientation to upwind in the presence of reward-predicting odor. Upwind steering of flies with blocked SMP108 (SS67221/UAS-TNT) was indistinguishable with control genotypes. N=15-16

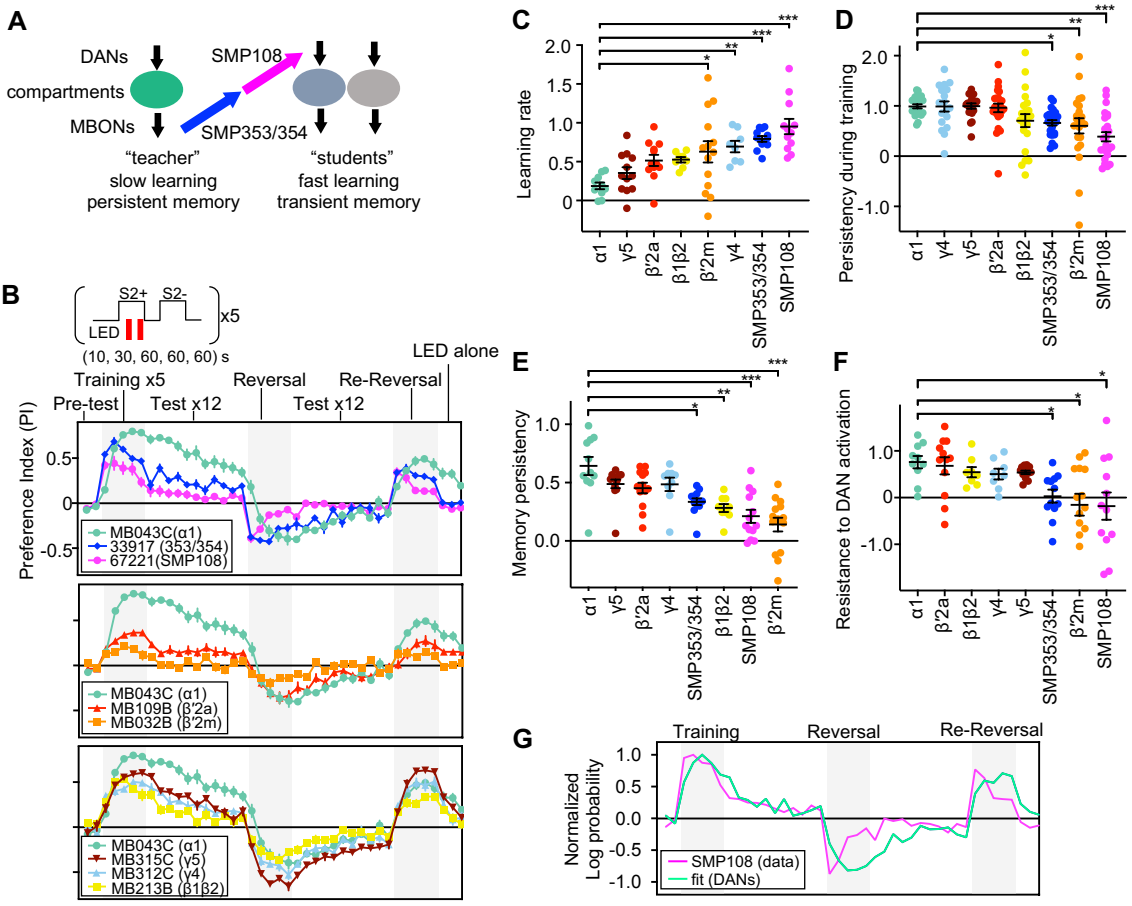

Figure 7 SMP108 pathway induces transient memory

(A) Teacher-student compartments model of second-order conditioning hypothesizes that "teacher" compartment with slow learning rate and persistent memory instructs other compartments with faster learning rate and transient memory dynamics via SMP353/SMP354 and SMP108.

(B) Dynamics of memory with optogenetic activation of SMP108 (SS67221), SMP353/354 (SS33917) or various types of DANs. See texts and methods for explanation of the protocol, and Figure 7-figure supplement 1 for specificity of expression pattern in the central brain and the ventral nerve cord. Means and SEM are displayed. N=8-14.

(C) Learning rate defined as a (PI after first 10s training)/(peak PI during the first 5 training trials) for each driver line.

(D) Persistency during training defined as (PI after 5th training)/(peak PI during the first 5 training trials).

(E) Persistency of memory defined as (mean of PIs during 12 tests after first training trials)/(peak PI during the first 5x training trials).

(F) Resistance to DAN activation defined as (mean of last three tests following activation LED without odors)/(PI after 5th conditioning in re-reversal phase), which measures both transiency during training and extinction during 12 tests. p<0.05; **, p<0.01; ***, p<0.01; Dunn's multiple comparison tests following Kruskal-Wallis test; N=8-14.

(G) The log-probability ratio of choosing the S2+ against S2- for SS67221 (SMP108) data were fitted best with weights of (0.57, 0.46,0.157,0,0,0) for data of DAN driver lines (MB032B, MB213B, MB312C, MB043C, MB109B and MB315C).

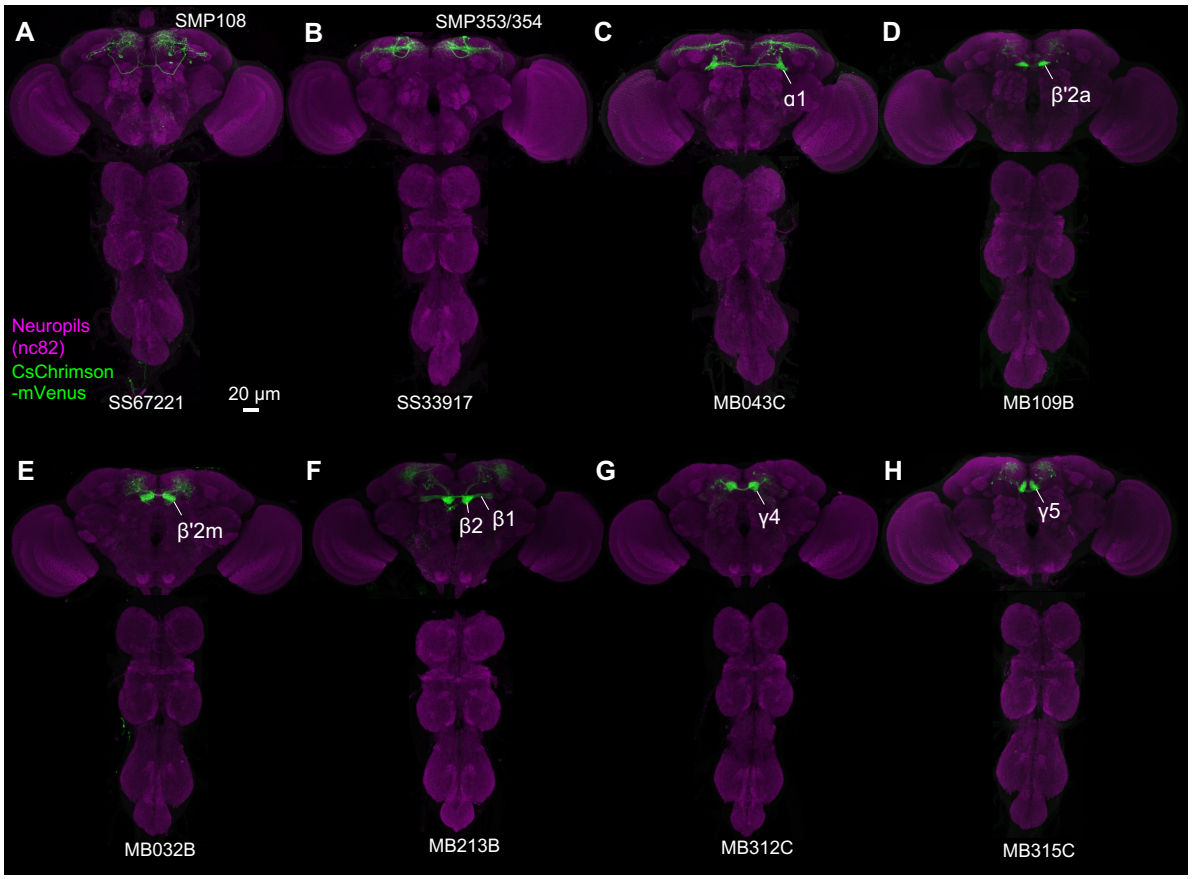

Figure 7-figure supplement 1 Expression patterns of CsChrimson
(A-H) Projection of confocal microscopy stacks for expression patterns of CsChrimson-mVenus driven by designated split-GAL4 driver lines in brains and ventral nerve cords. Confocal stacks are available at https://splitgal4.janelia.org